

Soft Photon Radiation in Particle Decays in SHERPA

M. SCHÖNHERR^{1a}, F. KRAUSS^{2b}

^a*Institut für Kern- und Teilchenphysik, TU Dresden, D-01062 Dresden, Germany*

^b*Institute for Particle Physics Phenomenology, Durham University, Durham DH1 3LE, UK*

ABSTRACT

In this paper the Yennie–Frautschi–Suura approach is used to simulate real and virtual QED corrections in particle decays. It makes use of the universal structure of soft photon corrections to resum the leading logarithmic QED corrections to all orders, and it allows a systematic correction of this approximate result to exact fixed order results from perturbation theory. The approach has been implemented as a Monte Carlo algorithm, which a posteriori modifies decay matrix elements through the emission of varying numbers of photons. The corresponding computer code is incorporated into the SHERPA event generator framework.

¹marek.schoenherr@tu-dresden.de

²frank.krauss@durham.ac.uk

Contents

1	Introduction	3
2	YFS-Exponentiation	4
3	The Algorithm	8
3.1	The master formula	8
3.2	Phase space transformation	10
3.3	Mapping of momenta	11
3.3.1	Neutral initial states: final state multipoles	11
3.3.2	Charged initial state: Mixed multipoles	12
3.4	Event generation	14
4	Higher Order Corrections	16
4.1	Approximations for real emission matrix elements	17
4.2	Exact real emission matrix elements	18
4.2.1	Two-body decays of type $V \rightarrow FF$	19
4.3	Virtual emission correction $\tilde{\beta}_0^1$	20
5	Results	21
5.1	Validation: leptonic heavy gauge boson decays	21
5.1.1	Radiated photon energy	21
5.1.2	Comparison with other codes	22
5.1.3	Effects of inclusion of exact matrix elements	25
5.2	Other channels	27
5.2.1	J/Ψ decays to leptons	27
5.2.2	$B \rightarrow D^* +$ pions and semileptonic B decays	28
5.2.3	$\Delta^{++} \rightarrow p^+ \pi^+$ decays	31
5.2.4	τ decays	31
6	Conclusions and outlook	31
A	The YFS-Form-Factor	34
A.1	Special cases	35
A.1.1	Two-body decay with $(p_i\theta_i + p_j\theta_j)^2 < 0$	35
A.1.2	Two-body decay with $(p_i\theta_i + p_j\theta_j)^2 = 0$	36
A.2	The full YFS form factor	36
B	Transforming the phase space elements	40
B.1	Rewriting the phase space element in other frames	40
B.2	Rewriting the phase space element in terms of the undressed momenta	42
B.2.1	Mixed multipoles	42
B.2.2	Final state multipoles	45

C	Details on the photon generation	47
C.1	Avarage photon multiplicity	47
C.2	Photon energy	49
C.3	Photon angles	49
C.4	Photons from multipoles	50
D	Massive dipole splitting functions	51
E	Basic building blocks For matrix element calculations	53

1 Introduction

The next round of collider-based experiments in particle physics will start with the LHC finally becoming fully operational, and producing particle collision data at unprecedented rate and energy. In the preparation for this huge enterprise, a new generation of Monte Carlo simulation tools, like PYTHIA8 [1], HERWIG++ [2] and SHERPA [3] has been constructed, to meet the increasingly complicated experimental situation and the demand for an improved description of data at a higher level of accuracy. In addition, it was anticipated that by moving to the new programming paradigm of object orientation and modularization the more mundane software management task of code validation and maintenance could be addressed in a more transparent and alleviated way. This leads to the typical strategy of event generators, to dissect the simulation of full events into different physics aspects, being better reflected in the modular structure of the emerging new codes.

In this paper the construction of a new physics module for the SHERPA framework is discussed, which deals with the simulation of QED radiation in particle decays. Up to now, this has typically been left to the PHOTOS [4,5] programme. However, there have been two reasons for replacing PHOTOS: First of all, PHOTOS builds on a parton-shower like collinear approximation for the simulation of photon emissions, which intrinsically has some shortcomings when the mass of the decaying particle is not much larger than the masses of its decay products. This has already been noted in [6,7] and triggered the development of the module SOPHTY [6] in the framework of the HERWIG++ event generator. It also has become a wide-spread belief among the authors of the main event generators that the maintenance of interface structures to additional codes such as PHOTOS, supplementing QED radiation to the simulation, overwhelms the burden of constructing and maintaining corresponding modules directly in the event generators.

Similar to the case of SOPHTY in HERWIG++, the construction of the new module, PHOTONS++, in SHERPA bases on the approach of Yennie, Frautschi and Suura (YFS) [8] for the calculation of higher order QED corrections to arbitrary processes. This approach resides on the idea of re-summing the leading soft logarithms to all orders, rather than focusing on the leading collinear terms. These soft logarithms are largely independent of the inner process characteristics and can be calculated from the external particles and their four-momenta only. The big advantage of the YFS formalism is that in addition it allows for a systematic improvement of this eikonal approximation, order-by-order in the QED coupling constant. This explains why a good fraction of the most precise tools for the simulation of QED radiation root in this algorithm [9,10,11,12].

In contrast to the SOPHTY implementation the aim of this implementation is to address also decays with more than two final state particles. This leads to different strategies of enforcing four-momentum conservation after the soft photons are reconstructed. In addition, some correction terms to restore precise results for the first order in the electromagnetic coupling constant are employed, improving the formal accuracy of the results of PHOTONS++. This also has not been included in SOPHTY.

The outline of this paper is as follows: After briefly reviewing the YFS formalism in Sec. 2 in the framework of particle decays, the Monte Carlo algorithm adopted here is detailed in Sec. 3. Then, some higher order corrections are discussed in Sec. 4. Finally, in Sec. 5 the new

code is validated through a detailed comparison with HORACE and WINDEC [13] for the case of leptonic Z and W decays before some results relating to other particle decays are presented.

2 YFS-Exponentiation

In this section, the YFS approach [8] for an approximative description of real and virtual QED corrections to arbitrary scattering or decay processes will shortly be reviewed, in the framework of particle decays. The virtue of this formalism is that it can systematically be improved, order by order in the electromagnetic coupling constant α . The YFS approach bases on the observation that the soft limits for matrix elements with real and/or virtual photons exhibit a universal behaviour, and on the fact that the corresponding soft divergences can be factorised into universal factors multiplying leading order matrix elements.

When defining the final state as a configuration of primary decay products with momenta p_f and any number of additional soft photons with momenta k the fully inclusive decay rate reads

$$\Gamma = \frac{1}{2M} \sum_{n_R=0}^{\infty} \frac{1}{n_R!} \int d\Phi_p d\Phi_k (2\pi)^4 \delta\left(\sum p_i - \sum p_f - \sum k\right) \left| \sum_{n_V=0}^{\infty} \mathcal{M}_{n_R}^{n_V + \frac{1}{2}n_R} \right|^2 \quad (1)$$

where p_i is the four-momentum of the decaying particle. Here and in the following n_V and n_R are the numbers of additional virtual and real photons, respectively, that show up in the higher-order matrix element but not in the uncorrected zeroth order matrix element (thus labelled by \mathcal{M}_0^0). The starting point of the YFS algorithm is to approximate these dressed matrix elements through the zeroth order one times eikonal factors, which depend on the external particles only. This effectively catches the leading logarithmic QED corrections to the process. The correct result can then be restored order by order in perturbation theory by supplementing the non-leading, process-dependent pieces.

In the case of one virtual photon this can be formalised as

$$\mathcal{M}_0^1 = \alpha B \mathcal{M}_0^0 + M_0^1, \quad (2)$$

where M_0^1 is the infrared-subtracted matrix element including one virtual photon (with M_0^1 finite when $k \rightarrow 0$ due to the subtraction). All soft divergences due to this virtual photon are contained in the process-independent, universal factor B , see Appendix A for a more thorough discussion. Here, and in the following, the sub- and superscripts denote the number of real photons and the order of α , respectively, both for the infrared-subtracted and for the original matrix elements.

Similar to the one-photon case, YFS showed that the subsequent insertion of further virtual photons in all possible ways leads to

$$\begin{aligned} \mathcal{M}_0^0 &= M_0^0 \\ \mathcal{M}_0^1 &= \alpha B M_0^0 + M_0^1 \\ \mathcal{M}_0^2 &= \frac{(\alpha B)^2}{2!} M_0^0 + \alpha B M_0^1 + M_0^2 \end{aligned} \quad (3)$$

and so on. Therefore, for a fixed order in α ,

$$\mathcal{M}_0^{n_V} = \sum_{r=0}^{n_V} M_0^{n_V-r} \frac{(\alpha B)^r}{r!} \quad (4)$$

and, summing over all numbers of virtual photons n_V ,

$$\sum_{n_V=0}^{\infty} \mathcal{M}_0^{n_V} = \exp(\alpha B) \sum_{n_V=0}^{\infty} M_0^{n_V}. \quad (5)$$

Since photons do not carry any charge and because virtual photons inserted in closed charged loops do not produce any additional infrared singularity¹, this can be generalised to any number of real photons, such that

$$\left| \sum_{n_V=0}^{\infty} \mathcal{M}_{n_R}^{n_V+\frac{1}{2}n_R} \right|^2 = \exp(2\alpha B) \left| \sum_{n_V=0}^{\infty} M_{n_R}^{n_V+\frac{1}{2}n_R} \right|^2. \quad (6)$$

Hence, $M_{n_R}^{n_V+\frac{1}{2}n_R}$ is free of soft singularities due to virtual photons but it still may contain those due to real photons.

YFS showed in [8] that the factorisation for real photon emission proceeds on the level of the squared matrix elements rather than on the amplitude level. For a single photon emission therefore this yields

$$\frac{1}{2(2\pi)^3} \left| \sum_{n_V=0}^{\infty} M_1^{n_V+\frac{1}{2}} \right|^2 = \tilde{S}(k) \left| \sum_{n_V=0}^{\infty} M_0^{n_V} \right|^2 + \sum_{n_V=0}^{\infty} \tilde{\beta}_1^{n_V+1}(k). \quad (7)$$

Here, $\tilde{S}(k)$ is an eikonal factor containing the soft divergence related to the real photon emission, see Appendix A. Denoting with $\tilde{\beta}_{n_R}^{n_V+n_R}$ the complete IR-finite (subtracted) squared matrix element for the basic process plus the emission of n_R photons including n_V virtual photons and using the abbreviation

$$\tilde{\beta}_{n_R} = \sum_{n_V=0}^{\infty} \tilde{\beta}_{n_R}^{n_V+n_R}, \quad (8)$$

the squared matrix element for n_R real emissions, summed over all possible virtual photon

¹ A similar program cannot directly be translated to QCD, where the emitted gluons act as parts of antennae emitting further gluons, thus modifying the pattern of possible infrared poles and thus leading logarithms in each emission.

corrections, can be written as

$$\begin{aligned}
& \left(\frac{1}{2(2\pi)^3} \right)^{n_R} \left| \sum_{n_V=0}^{\infty} M_{n_R}^{n_V + \frac{1}{2}n_R} \right|^2 \\
&= \tilde{\beta}_0 \prod_{i=1}^{n_R} \left[\tilde{S}(k_i) \right] + \sum_{i=1}^{n_R} \left[\frac{\tilde{\beta}_1(k_i)}{\tilde{S}(k_i)} \right] \prod_{j=1}^{n_R} \left[\tilde{S}(k_j) \right] + \sum_{\substack{i,j=1 \\ i \neq j}}^{n_R} \left[\frac{\tilde{\beta}_2(k_i, k_j)}{\tilde{S}(k_i)\tilde{S}(k_j)} \right] \prod_{l=1}^{n_R} \left[\tilde{S}(k_l) \right] + \dots \\
&+ \sum_{i=1}^{n_R} \left[\tilde{\beta}_{n_R-1}(k_1, \dots, k_{i-1}, k_{i+1}, \dots, k_{n_R}) \tilde{S}(k_i) \right] + \tilde{\beta}_{n_R}(k_1, \dots, k_{n_R}). \tag{9}
\end{aligned}$$

Demanding agreement with the exact result up to $\mathcal{O}(\alpha)$, this expression thus contains only terms with $\tilde{\beta}_0^0$, $\tilde{\beta}_0^1$ and $\tilde{\beta}_1^1$. Then

$$\begin{aligned}
& \left(\frac{1}{2(2\pi)^3} \right)^{n_R} \left| \sum_{n_V=0}^{\infty} M_{n_R}^{n_V + \frac{1}{2}n_R} \right|^2 \\
&= \left[\tilde{\beta}_0^0 + \tilde{\beta}_0^1 \right] \prod_{i=1}^{n_R} \left[\tilde{S}(k_i) \right] + \sum_{i=1}^{n_R} \left[\frac{\tilde{\beta}_1^1(k_i)}{\tilde{S}(k_i)} \right] \prod_{j=1}^{n_R} \left[\tilde{S}(k_j) \right] + \mathcal{O}(\alpha^2). \tag{10}
\end{aligned}$$

Inserting this into the expression for the decay rate and expressing the δ -functions ensuring four-momentum conservation as exponentials yields,

$$\begin{aligned}
2M \cdot \Gamma &= \sum_{n_R} \frac{1}{n_R!} \int d\Phi_{p_f} \left\{ \exp[2\alpha B] \int dy \exp \left[iy \left(\sum p_i - \sum p_f \right) \right] \right. \\
&\quad \left. \times \left(\int \frac{d^3k}{k} \tilde{S}(k) e^{-iyk} \right)^{n_R} \left(\tilde{\beta}_0^0 + \tilde{\beta}_0^1 \right) \right\} \\
&+ \sum_{n_R-1} \frac{1}{(n_R-1)!} \int d\Phi_{p_f} \left\{ \exp[2\alpha B] \int dy \frac{d^3K}{K} \exp \left[iy \left(\sum p_i - \sum p_f - K \right) \right] \right. \\
&\quad \left. \times \left(\int \frac{d^3k}{k} \tilde{S}(k) e^{-iyk} \right)^{n_R-1} \tilde{\beta}_1^1(K) \right\} + \mathcal{O}(\alpha^2) \\
&= \int d^4y \int d\Phi_{p_f} \left\{ \exp[2\alpha B] \exp \left[iy \left(\sum p_i - \sum p_f \right) + \int \frac{d^3k}{k} \tilde{S}(k) e^{-iyk} \right] \right. \\
&\quad \left. \times \left[\tilde{\beta}_0^0 + \tilde{\beta}_0^1 + \int \frac{d^3K}{K} e^{-iyK} \tilde{\beta}_1^1(K) + \mathcal{O}(\alpha^2) \right] \right\}. \tag{11}
\end{aligned}$$

As before, all singularities due to virtual photons are contained in B , while all singularities due to real emissions are incorporated in the integral over $\tilde{S}(k)$. To restore the momentum conserving δ -function the divergences have to be split off this integral. This can be done by simply subtracting the terms that are divergent for $k \rightarrow 0$. To this end, a small “soft” region Ω is defined together with an infrared-safe function $D(\Omega)^2$, such that

$$\begin{aligned} & \int \frac{d^3k}{k} \tilde{S}(k) e^{-iyk} \\ &= \int \frac{d^3k}{k} \left\{ \tilde{S}(k) \left[\left(1 - \Theta(k, \Omega)\right) + e^{-iyk} \Theta(k, \Omega) + \left(e^{-iyk} - 1\right) \left(1 - \Theta(k, \Omega)\right) \right] \right\} \\ &= 2\alpha \tilde{B}(\Omega) + D(\Omega) \end{aligned} \quad (12)$$

where

$$\begin{aligned} D(\Omega) &= \int \frac{d^3k}{k} \tilde{S}(k) \left[\left(e^{-iyk} - 1\right) \left(1 - \Theta(k, \Omega)\right) + e^{-iyk} \Theta(k, \Omega) \right] \\ &\xrightarrow{\Omega \rightarrow 0} \int \frac{d^3k}{k} \tilde{S}(k) e^{-iyk} \Theta(k, \Omega) \end{aligned} \quad (13)$$

and

$$2\alpha \tilde{B}(\Omega) = \int \frac{d^3k}{k} \tilde{S}(k) (1 - \Theta(k, \Omega)) = \int_{\Omega} \frac{d^3k}{k} \tilde{S}(k). \quad (14)$$

Reinserting this into the cross section, executing the y -integration and reexpanding the exponentiated integral yields

$$\begin{aligned} 2M \Gamma &= \sum_{n_R} \frac{1}{n_R!} \int d\Phi_{p_f} d\Phi'_k (2\pi)^4 \delta^4 \left(\sum p_i - \sum p_f - \sum k \right) e^{2\alpha(B + \tilde{B}(\Omega))} \\ &\quad \times \prod_{i=1}^{n_R} \tilde{S}(k_i) \Theta(k_i, \Omega) \left(\tilde{\beta}_0^0 + \tilde{\beta}_0^1 + \sum_{i=1}^{n_R} \frac{\tilde{\beta}_1^1(k_i)}{\tilde{S}(k_i)} + \mathcal{O}(\alpha^2) \right). \end{aligned} \quad (15)$$

The whole factorisation is independent of possible spin correlations in the “undressed” matrix element. Thus, the same result is obtained if the spin-summed and averaged matrix element squared $|\mathcal{M}|^2$ is replaced by $\rho_{\alpha\beta} \mathcal{M}^\alpha \mathcal{M}^{\beta*}$ where $\rho_{\alpha\beta}$ is a spin density matrix.

The infrared subtracted squared matrix elements read, up to $\mathcal{O}(\alpha)$,

$$\begin{aligned} \tilde{\beta}_0^0 &= M_0^0 M_0^{0*} \\ \tilde{\beta}_0^1 &= M_0^0 M_0^{1*} + M_0^1 M_0^{0*} \\ \tilde{\beta}_1^1 &= \frac{1}{2(2\pi)^3} M_1^{\frac{1}{2}} M_1^{\frac{1}{2}*} - \tilde{S}(k) M_0^0 M_0^{0*} \end{aligned} \quad (16)$$

² Obviously $\Theta(k, \Omega)$ divides the phase space into two regions. While Ω comprises the region containing the infrared divergence, $(1 - \Omega)$ is completely free of those divergences. Hence, $\Theta(k, \Omega) = 1$ if $k \notin \Omega$ and zero otherwise. Thus, $D(\Omega)$ is IR save and $\tilde{B}(\Omega)$ contains the divergence.

or

$$\begin{aligned}
\tilde{\beta}_0^0 &= \rho_{\alpha\beta} M_0^{0\alpha} M_0^{0\beta*} \\
\tilde{\beta}_0^1 &= \rho_{\alpha\beta} \left(M_0^{0\alpha} M_0^{1\beta*} + M_0^{1\alpha} M_0^{0\beta*} \right) \\
\tilde{\beta}_0^1 &= \rho_{\alpha\beta} \left(\frac{1}{2(2\pi)^3} M_1^{\frac{1}{2}\alpha} M_1^{\frac{1}{2}\beta*} - \tilde{S}(k) M_0^{0\alpha} M_0^{0\beta*} \right).
\end{aligned} \tag{17}$$

3 The Algorithm

3.1 The master formula

The basic, undressed matrix element (no additional photons) reads

$$2M \cdot \Gamma_0 = \int d\Phi_q (2\pi)^4 \delta^4(p_C + p_N - Q_C - Q_N) |\mathcal{M}|^2 \tag{18}$$

where the differential phase-space element for the outgoing momenta $q \in \{Q_C, Q_N\}$ is given by

$$d\Phi_q = \prod_{i=1}^n \frac{d^3q_i}{(2\pi^3)2q_i^0}. \tag{19}$$

Here, and in the following, the initial and final state momenta have been classified to whether the respective particles are charged or neutral: the sums of all initial state momenta are labelled by $p_{C,N}$ for charged and neutral particles, respectively, while $Q_{C,N}$ denotes the sums of all charged or neutral final state momenta. After QED corrections, the Q_C and Q_N will become P_C and P_N , respectively. K is the sum of all additional real, resolved Bremsstrahlungs-photons generated in the process, whereas photons already present in the core process are included in P_N and Q_N , respectively (an example for this seemingly unlikely case would be the rare decay $B^+ \rightarrow K^{*+}\gamma$).

In the previous section the factorisation of infrared divergent terms and the construction of infrared-finite expressions for cross sections with all possible numbers of resolved photons has been discussed. In these expressions the universal, process-independent parts of the QED corrections have been separated and exponentiated, the residual process dependence and the effect of particle spins etc. has been absorbed in infrared-finite, subtracted terms $\tilde{\beta}$, cf. Eq. (15). With small changes in the notation this form of the cross section thus reads

$$2M \cdot \Gamma = \sum_{n_\gamma} \frac{1}{n_\gamma!} \int d\Phi e^{Y(\Omega)} \prod_{i=1}^{n_\gamma} \tilde{S}(k_i) \Theta(k_i, \Omega) \tilde{\beta}_0^0 \mathcal{C}. \tag{20}$$

Here, the phase space has been separated into a phase space element for the particles of the ‘‘core’’ process and one for the additional n_γ resolved real photons,

$$d\Phi = d\Phi_p d\Phi_k (2\pi)^4 \delta(p_C + p_N - P_C - P_N - K). \tag{21}$$

with

$$d\Phi_p = \prod_{i=1}^n \frac{d^3 p_i}{(2\pi)^3 2p_i^0} \quad (22)$$

$$d\Phi_k = \prod_{i=1}^{n_\gamma} \frac{d^3 k}{k^0}. \quad (23)$$

Note that the factor $\frac{1}{2(2\pi)^3}$, missing in the photon phase space element, has already been incorporated in the eikonal factor $\tilde{S}(k)$, in accordance with the choice made in [8]. In the equation above, Eq. (20), the undressed matrix element $\tilde{\beta}_0^0$ has been factored out and the remainder of the perturbative expansion in α has been combined in the factor \mathcal{C} ,

$$\mathcal{C} = 1 + \frac{1}{\tilde{\beta}_0^0} \left(\tilde{\beta}_0^1 + \sum_{i=1}^{n_\gamma} \frac{\tilde{\beta}_1^1(k_i)}{\tilde{S}(k_i)} + \mathcal{O}(\alpha^2) \right). \quad (24)$$

Furthermore, the YFS-Form-Factor has been introduced

$$Y(\Omega) = \sum_{i < j} Y_{ij}(\Omega) = \sum_{i < j} 2\alpha \left(B_{ij} + \tilde{B}_{ij}(\Omega) \right) \quad (25)$$

where the sum $i < j$ runs over all pairs of charged particles, taking into account each pair only once. The infrared factors B_{ij} and \tilde{B}_{ij} are defined as

$$B_{ij} = -\frac{i}{8\pi^3} Z_i Z_j \theta_i \theta_j \int d^4 k \frac{1}{k^2} \left(\frac{2p_i \theta_i - k}{k^2 - 2(k \cdot p_i) \theta_i} + \frac{2p_j \theta_j + k}{k^2 + 2(k \cdot p_j) \theta_j} \right)^2 \quad (26)$$

$$\tilde{B}_{ij}(\Omega) = \frac{1}{4\pi^2} Z_i Z_j \theta_i \theta_j \int d^4 k \delta(k^2) (1 - \Theta(k, \Omega)) \left(\frac{p_i}{p_i \cdot k} - \frac{p_j}{p_j \cdot k} \right)^2. \quad (27)$$

They are the generalisation of the quantities defined in the last section, cf. Eqs. (2) and (14). Both contain the virtual and real infrared divergences, respectively. These divergences cancel according to the Kinoshita-Lee-Nauenberg theorem [14,15]. Thus, each $Y_{ij}(\Omega)$ is guaranteed to be finite, which is explicitly shown in Appendix A. In the terms above, Z_i and Z_j are the charges of the particles i and j in terms of the positron charge e , and the signature factors $\theta = \pm 1$ for particles in the final or initial state, respectively. The symbol Θ , already defined at the end of section 2, refers to a phase space constraint with Ω denoting the soft, unresolvable region of photon radiation. Hence, $\Theta(k, \Omega) = 1$ if $k \notin \Omega$ and zero otherwise. If this division is done by defining an energy cut-off, the definition of Ω is not Lorentz-invariant and the frame in which this cut-off forms a flat hypersurface also needs to be specified. The advantage of splitting the photon phase space in that manner lies in the alleviation of integrating $\tilde{S}(k)$ over k . If the cut-off is defined in the frame the photon generation and momentum reconstruction will be done in³ then the integration over the photon energy separates from the angular integration (see Appendix C), leading to yet another simplification of the calculation.

³ In the algorithm presented here, this will be the rest frame of the multipole, i.e. the combined rest frame of all charged particles $p_C + P_C$.

The eikonal factor $\tilde{S}(k)$ has already been introduced in the last section. It is defined as

$$\tilde{S}(k) = \sum_{i < j} \tilde{S}_{ij}(k) = \frac{\alpha}{4\pi^2} \sum_{i < j} Z_i Z_j \theta_i \theta_j \left(\frac{p_i}{p_i \cdot k} - \frac{p_j}{p_j \cdot k} \right)^2. \quad (28)$$

However, despite all terms being finite in Eq. (20), it cannot be used straight away for Monte Carlo generation. This is because it is written in terms of the already corrected final state momenta p_i and not the original undressed momenta q_i . The problem here is that the undressed momenta are defined in an n -body phase space whereas the dressed momenta are part of an $(n + n_\gamma)$ -body phase space. This necessitates a mapping procedure of the n -body onto the $(n + n_\gamma)$ -body phase space. In principle, details of this mapping procedure are irrelevant as long as it respects the soft limit of photon radiation not altering the original kinematics, i.e. in this limit the momenta of the original particles in the $(n + n_\gamma)$ -body phase space have to fall exactly onto those of the n -body phase space.

3.2 Phase space transformation

To solve this, consider the rest frame of all charged particles involved in the basic matrix element

$$P_M = p_C + P_C. \quad (29)$$

These particles form the multipole responsible for the Bremsstrahlung of the additional photons. In the rest frame of this multipole, a simple form of the mapping consists of a mere rescaling of the three-momenta of all final state particles by a common factor u such that the additional photons are accommodated. Clearly, the initial state momenta cannot be altered, because they have already been fixed when the basic matrix element was calculated. So, the task is to rewrite Eq. (21), explicitly in the rest frame of the multipole in question. The necessary transformations are detailed in the appendix, cf. App. B.1, here it suffices to give the result. It reads

$$\begin{aligned} d\Phi &= d\Phi_p d\Phi_k (2\pi)^4 \delta(p_C + p_N - P_C - P_N - K) \\ &= \prod_{i=1}^n \left[\frac{d^3 p_i}{(2\pi)^3 2p_i^0} \right] \prod_{i=1}^{n_\gamma} \left[\frac{d^3 k}{k^0} \right] (2\pi)^4 \delta(p_C + p_N - P_C - P_N - K) \\ &= d\Phi_p d\Phi_k \frac{m_{M,p}^3}{M^2(P_C^0 + P_N^0 + K^0)} (2\pi)^3 \delta^3(\vec{P}_M) (2\pi) \delta(P_M^0 - P_C^0 - p_C^0). \end{aligned} \quad (30)$$

In a similar fashion, the phase space related to the zeroth order uncorrected cross section can be transformed to

$$\begin{aligned} d\Phi_0 &= (2\pi)^4 d\Phi_q \delta^4(p_C + p_N - Q_C - Q_N) \\ &= \frac{m_{M,q}^3}{M^2(Q_C^0 + Q_N^0)} d\Phi_q (2\pi)^3 \delta^3(\vec{Q}_M) (2\pi) \delta(Q_M^0 - Q_C^0 - p_C^0). \end{aligned} \quad (31)$$

In both cases, $m_{M,p}$ ($m_{M,q}$) is the invariant mass of the corrected (uncorrected) multipole and the vector components P_C^0 and P_N^0 (Q_C^0 and Q_N^0) are taken in the P_M (Q_M) rest frame. The Jacobian emerging in both cases will ultimately find its way into a correction weight in the Monte Carlo realisation of the method.

3.3 Mapping of momenta

As mentioned before, the mapping procedure still has to be defined in detail to reconstruct the particles' momenta. The basic ideas of the mapping procedure suggested here are as follows: When representing all four-vectors in the rest frame of the multipole

- treat all final state momenta equally
- scale their three-momenta by a common factor u
- distribute the photon momenta
- assign the energy-component of every vector such that momentum conservation and all on-shell conditions are fulfilled

This will ultimately necessitate a change of the initial state momenta as well. However, since they are already fixed for the calculation of the basic matrix element this change will reduce to employing another frame during the reconstruction procedure.

However, closer examination reveals that the mapping paradigm above in fact enforces a different treatment for purely neutral and partially or fully charged initial state configurations. The reason is that the momenta of the newly generated Bremsstrahlungs photons need to be balanced. Furthermore, the phase space integral still has to be rewritten in terms of the undressed, original final state momenta defining the original matrix element and cross section without QED radiation. This will be addressed in the next sections, Sec. 3.3.1-3.3.2, where the case of decays, i.e. single initial state particles, either neutral or charged, will be discussed separately. Formally, of course, both treatments will yield identical results, since only the soft limit of photon emission is defined from first principles and because both treatments respect this limit.

3.3.1 Neutral initial states: final state multipoles

The first case to be considered is the case of a neutral particle of mass M decaying into a final state with charged particles. The reconstruction paradigm above completely fixes the reconstruction procedure to a rescaling of all final state momenta, both charged and neutral, and balancing the summed photon momentum K by moving the frame of the multipole and, hence, of the initial state⁴. Denoting, again, with q_i the undressed and with p_i the dressed final state momenta, and denoting their respective sums by Q_C , Q_N , P_C and P_N , as declared earlier, and using K as the summed momentum of all Bremsstrahlungs photons, the reconstruction prescription reads as follows:

⁴ Note that it is not possible to distribute any fraction of the photon momentum equally to all final states with the constraint that the multipole remains in its rest frame. It therefore is mandatory to balance the photon momentum with the initial state.

- The momenta of the Q_M rest frame

$$\begin{aligned}
p_N^\mu &= \left(\sqrt{M^2 + \vec{Q}_N^2}, \vec{Q}_N \right) \\
Q_C^\mu &= \left(Q_C^0, \vec{Q}_C = 0 \right) \\
Q_N^\mu &= \left(Q_N^0, \vec{Q}_N \right)
\end{aligned} \tag{32}$$

will be mapped onto

$$\begin{aligned}
p_N^\mu \longrightarrow p'_N{}^\mu &= \left(\sqrt{M^2 + (u\vec{Q}_N + \vec{K})^2}, u\vec{Q}_N + \vec{K} = u\vec{p}_N + \vec{K} \right) \\
P_C^\mu &= \left(P_C^0, u\vec{Q}_C = 0 \right)
\end{aligned} \tag{33}$$

$$P_N^\mu = \left(P_N^0, u\vec{Q}_N \right) \tag{34}$$

$$K^\mu = \left(K^0, \vec{K} \right) \tag{35}$$

in the P_M rest frame.

- p_N and p'_N are the same physical vector but in different frames. The scaling parameter u now is determined by momentum conservation, i.e.

$$0 = \sqrt{M^2 + (u\vec{Q}_N + \vec{K})^2} - \sum_C \sqrt{m_i^2 + u^2 \vec{q}_i^2} - \sum_N \sqrt{m_i^2 + u^2 \vec{q}_i^2} - K^0, \tag{36}$$

where the subscripts C and N in the sums indicate a summation over charged and neutral particles, respectively.

- The phase space element expressed in terms of the undressed final state momenta then reads

$$\begin{aligned}
d\Phi &= (2\pi)^4 d\Phi_q d\Phi_k \delta^3(\vec{Q}_M) \delta(Q_M^0 - Q_C^0 - p_C^0) \frac{m_{M,p}^3}{M^2 (P_C^0 + P_N^0 + K^0)} \\
&\times u^{3n-4} \frac{\frac{\vec{p}'_N{}^2}{p'_N{}^0} - \sum_{C,N} \frac{\vec{q}_i^2}{q_i^0}}{\frac{\vec{p}'_N \vec{p}'_N}{p'_N{}^0} - \sum_{C,N} \frac{\vec{p}_i \vec{q}_i}{p_i^0}} \prod_{i=1}^n \left[\frac{q_i^0}{p_i^0} \right].
\end{aligned} \tag{37}$$

3.3.2 Charged initial state: Mixed multipoles

The other case of relevance in the framework of this publication is the decay of a charged particle of mass M , leading to multipoles containing both initial and final state particles emitting the photons. Again the paradigm above completely fixes the reconstruction procedure. Basically, the problem is to compensate the photon momentum after the final state momenta have been rescaled. This is achieved in the following way:

- The momenta of the Q_M rest frame

$$\begin{aligned}
p_C^\mu &= \left(\sqrt{M^2 + \vec{Q}_C^2}, -\vec{Q}_C \right) \\
Q_C^\mu &= \left(Q_C^0, \vec{Q}_C \right) \\
Q_N^\mu &= \left(Q_N^0, \vec{Q}_N = -2\vec{Q}_C \right)
\end{aligned} \tag{38}$$

will be mapped onto

$$\begin{aligned}
p_C^\mu \longrightarrow p_c^{\mu'} &= \left(\sqrt{M^2 + (u\vec{Q}_C - n_C\vec{\kappa})^2}, -u\vec{Q}_C + n_C\vec{\kappa} = u\vec{p}_C + n_C\vec{\kappa} \right) \\
P_C^\mu &= \left(P_C^0, u\vec{Q}_C - n_C\vec{\kappa} \right) \\
P_N^\mu &= \left(P_N^0, u\vec{Q}_N - n_N\vec{\kappa} = -2u\vec{Q}_C - n_N\vec{\kappa} \right) \\
K^\mu &= \left(K^0, \vec{K} \right)
\end{aligned} \tag{39}$$

in the P_M rest frame. Here, n_C and n_N are the numbers of charged and neutral final state particles, respectively, and the abbreviation

$$\vec{\kappa} = \frac{1}{2n_C + n_N} \vec{K} \tag{40}$$

has been introduced for a more compact notation. Again, p_C and p_c' are the same physical vector represented in different frames, thus specifying the relation between the Q_M and the P_M rest frame. In the soft limit, i.e. for $K \rightarrow 0$, the scaling parameter $u \rightarrow 1$ and both vectors are identical, as required.

- In general, the scaling parameter is fixed through energy conservation as the solution of

$$0 = \sqrt{M^2 + (u\vec{Q}_C - n_C\vec{\kappa})^2} - \sum_C \sqrt{m_i^2 + (u\vec{q}_i - \vec{\kappa})^2} - \sum_N \sqrt{m_i^2 + (u\vec{q}_i - \vec{\kappa})^2} - K^0. \tag{41}$$

- The phase space integral rewritten in terms of the q_i reads

$$\begin{aligned}
d\Phi &= (2\pi)^4 d\Phi_q d\Phi_k \delta^3(\vec{Q}_M) \delta(Q_M^0 - Q_C^0 - p_C^0) \frac{m_{M,p}^3}{M^2 (P_C^0 + P_N^0 + K^0)} \\
&\times u^{3n-4} \frac{\frac{\vec{p}_C^2}{p_C^0} - \sum_{C,N} \frac{\vec{q}_i^2}{q_i^0}}{\frac{\vec{p}_C \vec{p}_C}{p_C^0} - \sum_{C,N} \frac{\vec{p}_i \vec{q}_i}{p_i^0}} \prod_{i=1}^n \left[\frac{q_i^0}{p_i^0} \right].
\end{aligned} \tag{42}$$

It is worth noting that this is identical to the case of a neutral particle in the initial state.

3.4 Event generation

Having transformed the phase space integrals allows to write the full decay rate including real and virtual QED radiation as

$$2M \cdot \Gamma = \sum_{n_\gamma} \frac{1}{n_\gamma!} \int d\Phi_q d\Phi_k (2\pi)^4 \delta^3(\vec{Q}_M) \delta(Q_M^0 - Q_C^0 - p_C^0) e^{Y(\Omega)} \tilde{\beta}_0^0 \mathcal{C} \\ \times \prod_{i=1}^{n_\gamma} \left[\tilde{S}(k_i) \Theta(k_i, \Omega) \right] \frac{m_{M,p}^3 u^{3n-4}}{M^2 (P_C^0 + P_N^0 + K^0)} \frac{\frac{\vec{p}^2}{p^0} - \sum_{C,N} \frac{\vec{q}_i^2}{q_i^0}}{\frac{\vec{p}'^2}{p'^0} - \sum_{C,N} \frac{\vec{p}_i \vec{q}_i}{p_i^0}} \prod_{i=1}^n \left[\frac{q_i^0}{p_i^0} \right], \quad (43)$$

where p and p' now generally stand for the initial state particle.

The zeroth order differential decay rate $d\Gamma_0$, which will be used by default in all decays in SHERPA can easily be extracted and, employing Eq. (31), reads

$$\Gamma = \sum_{n_\gamma} \frac{1}{n_\gamma!} \int d\Gamma_0 d\Phi_k e^{Y(\Omega)} \prod_{i=1}^{n_\gamma} \left[\tilde{S}(k_i) \Theta(k_i, \Omega) \right] \\ \times \frac{m_{M,p}^3}{m_{M,q}^3} \frac{Q_C^0 + Q_N^0}{P_C^0 + P_N^0 + K^0} u^{3n-4} \frac{\frac{\vec{p}^2}{p^0} - \sum_{C,N} \frac{\vec{q}_i^2}{q_i^0}}{\frac{\vec{p}'^2}{p'^0} - \sum_{C,N} \frac{\vec{p}_i \vec{q}_i}{p_i^0}} \prod_{i=1}^n \left[\frac{q_i^0}{p_i^0} \right] \mathcal{C}. \quad (44)$$

Up to here no approximations have been made at all. In order to generate the corresponding distribution with Monte Carlo techniques, however, this form is not particularly useful. To simplify Eq. (44) therefor, hit-or-miss and reweighting techniques are used, demanding upper bounds for the various pieces:

- All higher orders are neglected, thus setting \mathcal{C} to one.
- The maximum of all Jacobians is given for $K = 0$, coinciding with the leading-order phase space.
- The dependences on the dressed momenta in the eikonal factors are removed by approximating these factors by those depending on the undressed variables from the generation.

The resulting crude distribution reads

$$\Gamma_{\text{cr}} = \sum_{n_\gamma=0}^{\infty} \frac{1}{n_\gamma!} \int d\Gamma_0 d\Phi_k e^{Y(\omega)} \prod_{i=1}^{n_\gamma} \tilde{S}_q(k_i) \Theta(k_i, \Omega). \quad (45)$$

After executing all k -integrations giving

$$\int \prod_{i=1}^{n_\gamma} \frac{d^3 k_i}{k_i^0} \tilde{S}_q(k_i) \Theta(k_i, \Omega) = \bar{n}^{n_\gamma} \quad (46)$$

the YFS-Form-Factor is estimated by

$$Y(\Omega) \approx -\bar{n} \quad (47)$$

for suitable choices of Ω ⁵. Reinserting this into the crude estimate, the leading-order cross section can be separated from the QED radiation, and

$$\Gamma_{\text{cr}} = \Gamma_0 \sum_{n_\gamma=0}^{\infty} \left[\frac{1}{n_\gamma!} e^{-\bar{n}} \bar{n}^{n_\gamma} \right]. \quad (48)$$

The result is the undressed zeroth order cross section times a Poisson distribution with the average photon multiplicity \bar{n} . In this factorised state the photon distribution can be separated from the generation of the basic matrix element. Assuming the latter to be already generated it can *a posteriori* be corrected to the leading-logarithmic all-order QED correction by generating the photon distribution as follows:

1. Generate the number of photons according to a Poissonian distribution with mean \bar{n} .
2. Generate each photon's momentum according to $\tilde{S}_q(k)$. This implies
 - that its energy k^0 is distributed according to

$$\rho(k^0) \sim \frac{1}{k^0} \quad (49)$$

- and that the azimuthal and polar angles are distributed according to

$$\rho(\theta, \phi) \sim \sum_{i < j} \left(\frac{q_i}{q_i \cdot e_k} - \frac{q_j}{q_j \cdot e_k} \right)^2, \quad (50)$$

where e_k is a null vector of unit length,

$$e_k^\mu = \frac{1}{k^0} k^\mu \quad \text{with} \quad e_k^2 = 0. \quad (51)$$

It is possible that more than one hard photon is created such that the total energy of all photons exceeds the decaying system's energy. Obviously, this has to be avoided to guarantee energy conservation. A simple way of achieving this is a mere veto on such situations, accompanied with a repetition of photon generation, starting from step 1.

3. Reconstruct the momenta.
4. Calculate and apply all weights. This yields a total weight, namely

$$W = W_{\text{dipole}} \times W_{\text{YFS}} \times W_{\text{J,L}} \times W_{\text{J,M}} \times W_{\text{C}}, \quad (52)$$

⁵ In this publication (and in the code), this choice has been to limit the photon energies by setting an infrared energy cut-off of 0.1GeV, unless otherwise stated.

where the individual weights are given by

$$W_{\text{dipole}} = \prod_{i=1}^{n_\gamma} \frac{\tilde{S}(p_C, P_C, k_i)}{\tilde{S}(p_C, Q_C, k_i)} \quad (53)$$

$$W_{\text{YFS}} = \exp(Y(p_C, P_C, \Omega) + \bar{n}) \quad (54)$$

$$W_{\text{J,L}} = \frac{m_{M,p}^3}{m_{M,q}^3} \frac{Q_C^0 + Q_N^0}{P_C^0 + P_N^0 + K^0} \quad (55)$$

$$W_{\text{J,M}} = u^{3n-4} \frac{\frac{\vec{p}^2}{p^0} - \sum_{C,N} \frac{\vec{q}_i^2}{q_i^0}}{\frac{\vec{p}' \cdot \vec{p}}{p'^0} - \sum_{C,N} \frac{\vec{p}_i \cdot \vec{q}_i}{p_i^0}} \prod_{i=1}^n \left(\frac{q_i^0}{p_i^0} \right) \quad (56)$$

$$W_{\mathcal{C}} = \mathcal{C}. \quad (57)$$

Here, W_{dipole} corrects the emitting dipoles from the unmapped to the mapped momenta, W_{YFS} accounts for the exact YFS form factor, $W_{\text{J,L}}$ essentially denotes the Jacobian due to the Lorentz-transformation, $W_{\text{J,M}}$ is the weight due the momenta-mapping, and $W_{\mathcal{C}}$ incorporates higher-order corrections, where available.

The maximum of the combined weight indeed is smaller than the maximal weight employed for generating the distribution, $W < W(K = 0)$. Hence application of the combined weight is just a realisation of a hit-or-miss method. The distribution obtained is now the exact distribution of (20) or (44).

4 Higher Order Corrections

In the last section, the procedure generating the QED corrections to cross sections, following Eq. (15), has been outlined. By construction, the algorithm yields exact all-orders results, if all matrix elements are known. This, however, is never the case. On the other hand, the dominant universal soft photon contributions, real and virtual, are included to all orders in the YFS form factor, Eq. (25). Thus, if the zeroth order undressed matrix element only is known, i.e. if $\mathcal{C} = 1$, the photons will be solely generated according to a product of eikonal factors $\tilde{S}(k_i)$. Consequently, their distribution will be correct in the soft limit only. Away from this limit, exact matrix elements at a given order may be mandatory to yield satisfactory and sufficient accuracy. For most applications on decay matrix elements - the topic of this publication - it will be sufficient to implement the matrix element correction to the first order in α , i.e. for the emission of one additional real or virtual photon. It should be noted here that hard photon emission predominantly occurs in situations where potential emitters are characterised by a large energy-to-mass ratio and that in any case hard photon emissions tend to populate regions in phase space that are collinear w.r.t. the emitters. In contrast, large angle radiation has the tendency to be predominantly soft.

4.1 Approximations for real emission matrix elements

As already explained, the vast majority of hard photon emissions deserving an improved description through corrections to the soft limit underlying the YFS approach occurs in the collinear region of emission phase space. In this region, the well-known collinear factorisation can be used to approximate $\tilde{\beta}_1^1$. This amounts to an inclusion of the leading collinear logarithms arising in this limit, which are incorporated for instance in the Altarelli-Parisi evolution equation [16] and corresponding splitting kernels.

Since masses are to be taken fully into account the quasi-collinear limit defined in [17,18] replaces the more familiar collinear one. In this limit the matrix element factorises as

$$\sum_{\lambda_\gamma} \left| \mathcal{M}_1^{\frac{1}{2}}(p_i, k) \right|^2 \cong \begin{cases} e^2 Z_i^2 g^{(\text{out})}(p_i, k) |\mathcal{M}_0^0(p_i + k)|^2 & \text{if } i \in \text{F.S.} \\ e^2 Z_i^2 g^{(\text{in})}(p_i, k) |\mathcal{M}_0^0(x \cdot p_i)|^2 & \text{if } i \in \text{I.S.} \end{cases} \quad (58)$$

Here the $g^{(\text{in},\text{out})}(p_i, k)$ denote massive splitting functions. For instance, for the case of a fermion emitting a photon they are given by

$$g^{(\text{out})}(p_i, k) = \frac{1}{(p_i \cdot k)} \left(P_{ff}(z) - \frac{m_i^2}{(p_i \cdot k)} \right) \quad (59)$$

$$g^{(\text{in})}(p_i, k) = \frac{1}{x(p_i \cdot k)} \left(P_{ff}(x) - \frac{x m_i^2}{(p_i \cdot k)} \right), \quad (60)$$

where $x = \frac{p_i^0 - k^0}{p_i^0}$ and $z = \frac{p_i^0}{p_i^0 + k^0}$ are the fractions of the fermion energies kept after the emission of the photon, and where $P_{ff}(y)$ is the well-known Altarelli-Parisi splitting function

$$P_{ff}(y) = \frac{1 + y^2}{1 - y}. \quad (61)$$

The dipole splitting functions of [17] have been generalised further in [19] to incorporate also polarisation. Thus, in principle they could directly be used in the framework of the YFS formulation replacing the original eikonal factors. In the framework of this publication, however, they are employed as universal correction factors, reweighting explicit photon emission such that the correct collinear limit is recovered. Since they interpolate smoothly between both limits they already include the soft limit. Therefore, in the correction weights, these soft terms have to be subtracted because they are already accounted for in the original YFS eikonals. In addition, since the dipole splitting kernels refer to an emitter and a spectator forming the dipole, for each dipole two such terms have to be applied, such that the squared matrix element with the dipole terms approximating the photon emission reads

$$\left| \mathcal{M}_1^{\frac{1}{2}} \right|^2 \cong -e^2 \sum_{i \neq j} \left[Z_i Z_j \theta_i \theta_j g_{ij}(p_i, p_j, k) |\mathcal{M}_0^0|^2 \right] \quad (62)$$

$$\cong -e^2 \sum_{i < j} \left[Z_i Z_j \theta_i \theta_j (g_{ij}(p_i, p_j, k) + g_{ji}(p_j, p_i, k)) |\mathcal{M}_0^0|^2 \right]. \quad (63)$$

Here, charge conservation in the form $\sum Z_i \theta_i = 0$ has been used. The second particle in each massive splitting function g_{ij} denotes the spectator of the emission process and accounts for the recoil, thus ensuring four-momentum conservation. It should also be noted that the sum in the equations above runs over charged particles only.

In order to subtract the soft terms, it is useful to consider the soft and quasi-collinear limits of the dipole splitting kernels $g_{ij}(p_i, p_j, k)$:

$$g_{ij}(p_i, p_j, k) \stackrel{k \rightarrow 0}{\sim} \frac{1}{(p_i \cdot k)} \left(\frac{2(p_i \cdot p_j)}{(p_i \cdot k) + (p_j \cdot k)} - \frac{m_i^2}{(p_i \cdot k)} \right) \quad (64)$$

$$g_{ij}(p_i, p_j, k) \stackrel{p \cdot k \rightarrow 0}{\sim} g^{(\text{out/in})}. \quad (65)$$

Because the soft limit is universal and spin-independent, it is a straightforward exercise to define soft-subtracted dipole splitting kernels

$$\begin{aligned} \bar{g}_{ij}(p_i, p_j, k) &= g_{ij}(p_i, p_j, k) - g_{ij}^{(\text{soft})}(p_i, p_j, k) \\ &= g_{ij}(p_i, p_j, k) - \frac{1}{(p_i \cdot k)} \left(\frac{2(p_i \cdot p_j)}{(p_i \cdot k) + (p_j \cdot k)} - \frac{m_i^2}{(p_i \cdot k)} \right). \end{aligned} \quad (66)$$

The soft-subtracted dipole splitting kernels \bar{g}_{ij} now have the correct (finite) soft limit while retaining the original quasi-collinear limit of g_{ij} (Eq. (65)). Accordingly, the soft-subtracted matrix element can be approximated as

$$\tilde{\beta}_1^1 = -\frac{\alpha}{4\pi^2} \sum_{i < j} Z_i Z_j \theta_i \theta_j (\bar{g}_{ij}(p_i, p_j, k) + \bar{g}_{ji}(p_j, p_i, k)) \tilde{\beta}_0^0. \quad (67)$$

The exact form of the $g_{ij}(p_i, p_j, k)$ for different emitter-spectator configurations will be given in Appendix D.

4.2 Exact real emission matrix elements

In order to achieve an even higher precision, the implementation of exact higher-order full matrix elements becomes mandatory. It should be clear, however, that large differences with the approximated matrix elements above will occur only in non-singular regions of comparable hard, wide-angle emissions. Since the module presented in this publication, PHOTONS++, is embedded in the SHERPA framework it is easy to implement such infrared subtracted squared matrix elements, making use of tools and functions already provided within the framework. In particular, some basic building blocks for the calculation of helicity amplitudes already used in [20,21] can be recycled to construct the necessary, infrared-subtracted one-photon real emission matrix elements, which are then evaluated at momentum configurations generated by the algorithm of Section 3. These building blocks are listed in App. E. Exact first-order matrix elements have so been implemented for a number of relevant matrix elements, see below. It is worthwhile to stress that in principle also second-order precision could be achieved, if necessary.

In general, the infrared-subtracted squared matrix element can be written as

$$\tilde{\beta}_1^1 = \frac{1}{2(2\pi)^3} \mathcal{M}_1^{\frac{1}{2}} \mathcal{M}_1^{\frac{1}{2}*} - \tilde{S}(k) \mathcal{M}_0^0 \mathcal{M}_0^{0*}, \quad (68)$$

and it is only the amplitudes \mathcal{M} that are process-specific and need to be listed for the different processes. It should be noted that within the SHERPA framework the real emission matrix elements are straightforward to implement, in contrast, the incorporation of loop matrix elements is somewhat more involved: in those cases the integral has to be calculated analytically and the divergences must be cancelled before implementation as a function of the outer momenta.

4.2.1 Two-body decays of type $V \rightarrow FF$

The matrix elements for two body decays where one neutral vector particle decays into two charged fermions, $V \rightarrow FF$, read⁶

$$\begin{aligned}\mathcal{M}_0^0 &= ie \varepsilon_\mu^V(p, \lambda) \bar{u}(q_1, s_1) \gamma^\mu (c_L P_L + c_R P_R) v(q_2, s_2) \\ \mathcal{M}_1^{\frac{1}{2}} &= ie^2 \varepsilon_\mu^V(p, \lambda) \bar{u}(p_1, s_1) \left[\gamma^\nu \frac{\not{p}_1 + \not{k} + m}{(p_1 + k)^2 - m^2} \gamma^\mu (c_L P_L + c_R P_R) \right. \\ &\quad \left. - \gamma^\mu (c_L P_L + c_R P_R) \frac{\not{p}_2 + \not{k} - m}{(p_2 + k)^2 - m^2} \gamma^\nu \right] v(q_1, s_1) \varepsilon_\nu^*(k, \kappa). \quad (69)\end{aligned}$$

Of course, momentum conservation must hold, and therefore $p = q_1 + q_2$ in the former and $p = p_1 + p_2 + k$ in the latter case. Hence, if n_γ of the generated event exceeds the number of real photons in the respective infrared subtracted squared matrix element, a projection of the higher dimensional phase space onto the lower dimensional one has to be performed. In practise, this amounts to redoing the reconstruction procedure using only a subset of all photons generated in that run. Furthermore,

$$c_L P_L + c_R P_R = c_L \frac{1 - \gamma^5}{2} + c_R \frac{1 + \gamma^5}{2}. \quad (70)$$

Thus, the generic matrix element is adjustable to various decays of neutral vector bosons. A few key examples of the couplings c_L and c_R to the left and right-handed fermionic currents are listed in Table 1.

The real-emission matrix elements depend on the polarisations, and they are expressed in terms of the X , Y and Z functions listed in Appendix E as

$$\mathcal{M}_0^0 = ie X(q_1, s_1; \varepsilon^V; q_2, \bar{s}_2; c_L, c_R) \quad (71)$$

⁶ All particles involved are considered to be point-like, i.e. their vertices do not contain form factors.

Process	c_L	c_R
$Z \rightarrow \ell\ell$	$\frac{ie}{2s_W c_W} 2s_W^2$	$\frac{ie}{2s_W c_W} (2s_W^2 - 1)$
$J/\psi \rightarrow \ell\ell$	$-ie$	$-ie$

Table 1: Values of the coupling constants of different vector particles to the left- and right-handed leptonic currents.

and

$$\begin{aligned}
\mathcal{M}_1^{\frac{1}{2}} = & \\
& ie^2 \left[\frac{1}{2(p_a^2 - m^2)} \left(1 + \frac{m}{\sqrt{p_a^2}} \right) \sum_s X(p_1, s_1, \varepsilon^{\gamma^*}, p_a, s, 1, 1) X(p_a, s, \varepsilon^V, p_2, \bar{s}_2, c_L, c_R) \right. \\
& + \frac{1}{2(p_a^2 - m^2)} \left(1 - \frac{m}{\sqrt{p_a^2}} \right) \sum_s X(p_1, s_1, \varepsilon^{\gamma^*}, p_a, \bar{s}, 1, 1) X(p_a, \bar{s}, \varepsilon^V, p_2, \bar{s}_2, c_L, c_R) \\
& - \frac{1}{2(p_b^2 - m^2)} \left(1 + \frac{m}{\sqrt{p_b^2}} \right) \sum_s X(p_1, s_1, \varepsilon^V, p_b, s, c_L, c_R) X(p_b, s, \varepsilon^{\gamma^*}, p_2, \bar{s}_2, 1, 1) \\
& \left. - \frac{1}{2(p_b^2 - m^2)} \left(1 - \frac{m}{\sqrt{p_b^2}} \right) \sum_s X(p_1, s_1, \varepsilon^V, p_b, \bar{s}, c_L, c_R) X(p_b, \bar{s}, \varepsilon^{\gamma^*}, p_2, \bar{s}_2, 1, 1) \right] \quad (72)
\end{aligned}$$

where

$$\begin{aligned}
p_a &= p_1 + k \\
p_b &= p_2 + k,
\end{aligned} \quad (73)$$

and where p_1 and p_2 are the momenta of the final state leptons. The bar over the fermion spin label s_i signifies an anti-particle.

4.3 Virtual emission correction $\tilde{\beta}_0^1$

The only virtual corrections occuring to level $\mathcal{O}(\alpha)$ are

$$\begin{aligned}
\tilde{\beta}_0^1 &= M_0^1 M_0^{0*} + M_0^0 M_0^{1*} \\
&= \mathcal{M}_0^1 \mathcal{M}_0^{0*} + \mathcal{M}_0^0 \mathcal{M}_0^{1*} - 2\alpha B \tilde{\beta}_0^0.
\end{aligned} \quad (74)$$

For the above case of decays of the type $V \rightarrow FF$ they read

$$\tilde{\beta}_0^1 = \frac{\alpha}{\pi} \left[\ln \frac{m_V^2}{m_F^2} - A \right] \tilde{\beta}_0^0 \quad m_V^2 \gg m_F^2, \quad (75)$$

with

$$A = \begin{cases} 1 & \text{in on-shell scheme} \\ \frac{7}{4} & \text{in } \overline{MS} \text{ scheme} \end{cases} \quad (76)$$

which agrees with [22,23]. Effects of potentially different left- and right-handed couplings c_L and c_R , cf. Tab.1, only enter in terms suppressed by $\frac{m_F^2}{m_V^2}$ and are currently neglected in PHOTONS++.

For the process $W \rightarrow l\nu$, cf. [24], the first order virtual correction reads

$$\tilde{\beta}_0^1 = \frac{\alpha}{\pi} \left[\ln \frac{m_W}{m_\ell} + \frac{1}{2} \right] \tilde{\beta}_0^0 \quad m_W^2 \gg m_\ell^2. \quad (77)$$

5 Results

In this section some of the results of the PHOTONS++ module, as it is implemented within the SHERPA framework, are presented. The focus lies on the central distribution produced by the preceding calculations, the total energy of **all** photons radiated per event in the rest frame of the decaying particle. In addition, angular distributions for dipole and multipole configurations will be shown.

5.1 Validation: leptonic heavy gauge boson decays

The leptonic decays of W and Z bosons, $W \rightarrow l\nu_l$ and $Z \rightarrow \bar{l}l$, will play the central role in validating the accuracy of the PHOTONS++ implementation of the YFS approach. Before studying in more detail these processes and comparing the results obtained with PHOTONS++ with those from other codes, namely AMEGIC++ [20] and WINDEC [24], it is worthwhile to discuss one of the key distributions, namely the total energy radiated off the decay.

5.1.1 Radiated photon energy

The result for this distribution, namely the total energy radiated off the decay in form of photons, is presented in Figure 1. For both processes, i.e. for both leptonic Z and W decays, different leptons with different masses have been considered. Clearly, radiation is most important in final states involving electrons, being the lightest fermions taken into account, while radiation off heavier fermions is increasingly suppressed. One of the most prominent features of every radiated energy spectrum is the kink at around half the boson mass, which is due to kinematics. It limits the energy involved in single photon emission off the final state fermion to its maximal energy, roughly half the boson mass. This kink gets washed out and moves to the left with increasing fermion mass. Events with total radiated energy surpassing this limit must involve at least two sufficiently hard photons, arranged such that they recoil, at least partially, against each other. Naively, in the classical limit, such configurations are dominated by photon emission off both fermions. This motivates why radiation beyond the kink is absent in the W -decay spectra. Along the same lines of reasoning, such double hard photon emissions are decreasingly probable with rising lepton masses. However, since in the present state only approximated matrix elements up to $\mathcal{O}(\alpha)$ are included in the program these double emissions are not described correctly yet.

In Fig. 1 also different treatments of higher order matrix elements are exhibited: photons emitted solely according to the purely soft YFS eikonals (left panel) are contrasted with correc-

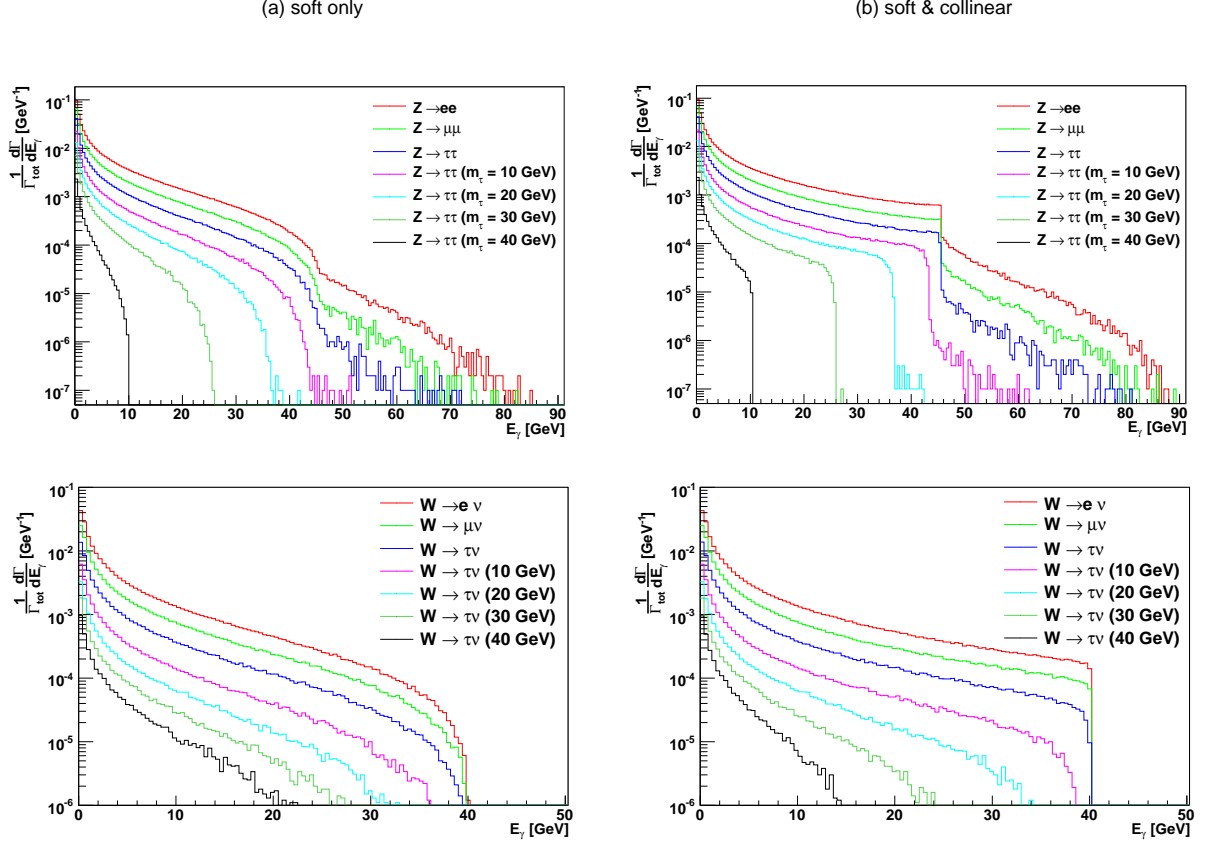


Figure 1: *Photon radiation in leptonic decays of Z (upper panel) and W bosons (lower panel) for different leptons, including fictional heavy τ 's in a range of masses. In the left panel, (a), $\mathcal{C} = 1$, i.e. photon generation according to the YFS form factor only is depicted, whereas in the right panel, (b), corrections up to $\mathcal{O}(\alpha)$ are included using the dipole splitting functions and the virtual corrections, cf. Sec. 4.3 and 4.1. All distributions are normalised on the total decay width of the decay into the respective lepton and lepton-neutrino pair. The infrared cut-off in all cases is set to 0.1GeV.*

tions due to the approximated matrix elements presented in Sec. 4.1. The former distribution, labelled with “soft”, thus is correct in the soft limit but it is inadequate for the description of hard, collinear photon radiation. This, including virtual corrections of $\mathcal{O}(\alpha)$, is displayed in the panel labelled with “soft & collinear”.

The inclusion of these corrections gives reasonably good results as long as most photons are soft or if complicated correlations of hard photons are not important.

5.1.2 Comparison with other codes

After checking the physical sanity of the implementation in principle, results obtained with PHOTONS++ are now to be compared to those from other, established and dedicated Monte

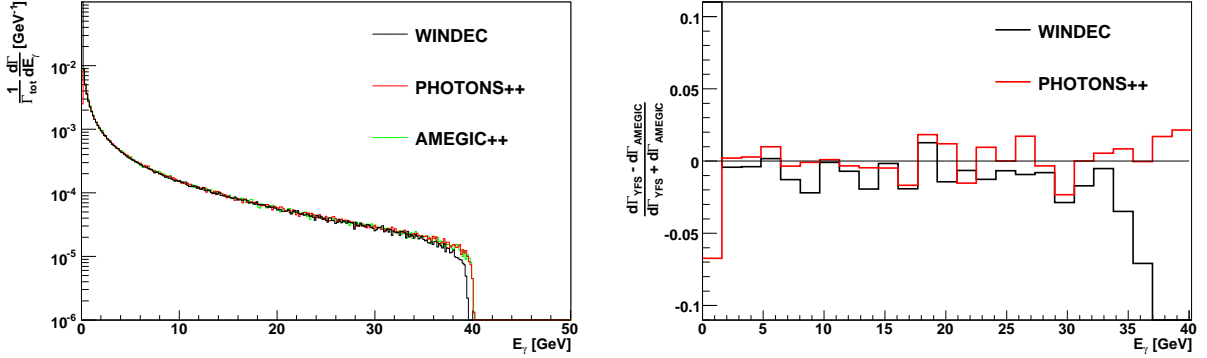


Figure 2: *The total photon energy in the decay frame in $W \rightarrow \tau\nu_\tau$. In the left panel, (a), the distributions generated by WINDEC (black), PHOTONS++ (red) and AMEGIC++ (green) are depicted, where the latter has been rescaled with the true average photon multiplicity. In the right panel, the relative deviations of WINDEC (black) and PHOTONS++ (red) with respect to the rescaled matrix element result of AMEGIC++ are displayed.*

Carlo event generators capable of describing QED effects in the decays of W and Z bosons, in particular with the WINDEC package [24]. This program aims at the description of the production and decay of W -bosons in hadronic collisions. WINDEC performs the decay of the W -boson into lepton-neutrino pairs including QED corrections summed in the YFS-approach and corrected by exact $\mathcal{O}(\alpha)$ real emission and virtual correction matrix elements. They are obtained for the decay only in the narrow width approximation, i.e. only the $W \rightarrow \ell\nu$ decay is taken into account. Furthermore, in this section, the results of PHOTONS++ are compared with the exact, fixed order, one-photon emission results of the SHERPA-inherent matrix element generator AMEGIC++. However, comparisons with AMEGIC++ are only sensible when the average photon number of the process under consideration is low, i.e. when multiphoton emission gives a negligible contribution to the differential cross section. Additionally, it should be stressed that AMEGIC++ lacks virtual corrections and therefore comparisons are sensible for normalised distributions only.

The channel best suited for comparing all three generators is $W \rightarrow \tau\nu_\tau$. Besides the low average photon multiplicity (with an infrared cut-off of 0.1 GeV multiphoton events make up for less than 3% of all radiative events) virtual corrections merely amount to a 1% correction of the zeroth order cross section. Furthermore, as discussed earlier, the majority of multiphoton events will consist of at most one single hard photon and additional soft ones. Therefore, these events will be approximately described by the hard emission only.

It should be stressed at this point, however, that there is one fundamental difference in the comparison of the various results, related to the way the infrared cut-off is implemented: While in WINDEC the energy cut-off is applied in the rest frame of the decaying W , it is applied in the rest-frame of the decaying dipole in both PHOTONS++ and AMEGIC++.

The distributions generated by all three programs are shown in Fig. 2. In general terms,

the distributions agree reasonably well with each other. There is, however, a slight deviation in the region of large radiated energies, where WINDEC undershoots the results of the two other codes on the level of up to 10%. On the other hand, WINDEC exhibits an overshoot in the very low energy bins, for radiated energies around or smaller 5 GeV, which is due to the different frames in which the infrared cut-offs are applied. As already mentioned, in WINDEC this is defined in the W rest frame, hence resulting in a flat hypersurface in this frame. In contrast, in PHOTONS++ it is applied in the rest frame of the W - l -dipole. Subsequently the surface of the region cut off by this definition forms a directionally dependent hypersurface in the rest frame of the W (observable in Fig. 3 where the cut-off is set to 1GeV). The net result is that some photons having more than 0.1GeV in this frame had less than 0.1GeV in the rest frame of the dipole, and vice versa. Ultimately, different definitions of the infrared cut-off result in different behaviour in the vicinity of this cut-off in nearby frames. The differences are the larger the further both frames are apart. On the other hand, the differences at high photon energies most likely stem from different mapping procedures in both codes. The mapping procedure in PHOTONS++, cf. Sec. 3.3.2, does not involve neutral particles, in this case the neutrino. It therefore ensures that the full phase space possible for the radiative decay can be mapped onto the leading order one.

Another feature to study is the dependence of the distributions on the choice of the infrared cut-off ω . It is employed to separate the divergent region of real soft photon emission, which is exponentiated together with the virtual contributions, from the region of the phase space where resolvable photons will be generated. Accordingly, this cut-off sets a limit on the number of photons to be generated. In Figure 3 the results of this variation on the spectrum of the radiated photons' total energy are exhibited for two different final states, electrons (upper panel) and τ 's (lower panel). In the case of the decays $W \rightarrow \tau\nu$ the two codes, PHOTONS++ (left panel) and WINDEC (right panel) show a similar behaviour: Varying the cutoffs between 1 MeV and 1 GeV yields stable results in large regions and especially also in the high-energy tail of the distribution, whereas differences appear only in the region of small energies, around 1-2 GeV. However, in the case of the decays $W \rightarrow e\nu$ the differences between the two codes are more pronounced. Varying the cutoff there yields still comparably stable results for PHOTONS++, but the results of WINDEC show a significant dependence on the cut-off of the order of around 10%. This is due to the fact that with decreasing fermion mass the effect of the infrared cutoff on the average photon number increases⁷.

In order to choose an optimal value of the infrared cut-off ω there are different considerations to be taken into account: On the one hand an efficient generation is desirable, pushing ω as high as physically sensible, e.g. the detector level energy resolution on soft photons or decay products. Along the same lines it should be noted that all photons in the soft (unresolved) region will be assumed to yield a negligible combined momentum. Therefore, choosing a comparably large infrared cut-off will not have any effect on distributions involving the resolved Bremsstrahlung photons, but it will reduce the accuracy of results obtained for e.g. invariant masses of the primary decay products. This consideration clearly demands a smaller cut-off. On the other hand, when exponentiating the real soft photon emission a factor $\int \frac{d^3k}{k^0} \tilde{S}(k)(e^{-iyk} - 1)\Theta(\omega - k^0)$

⁷ In fact, this feature was one of the reasons for preferring the τ decay channel over the electron channel.

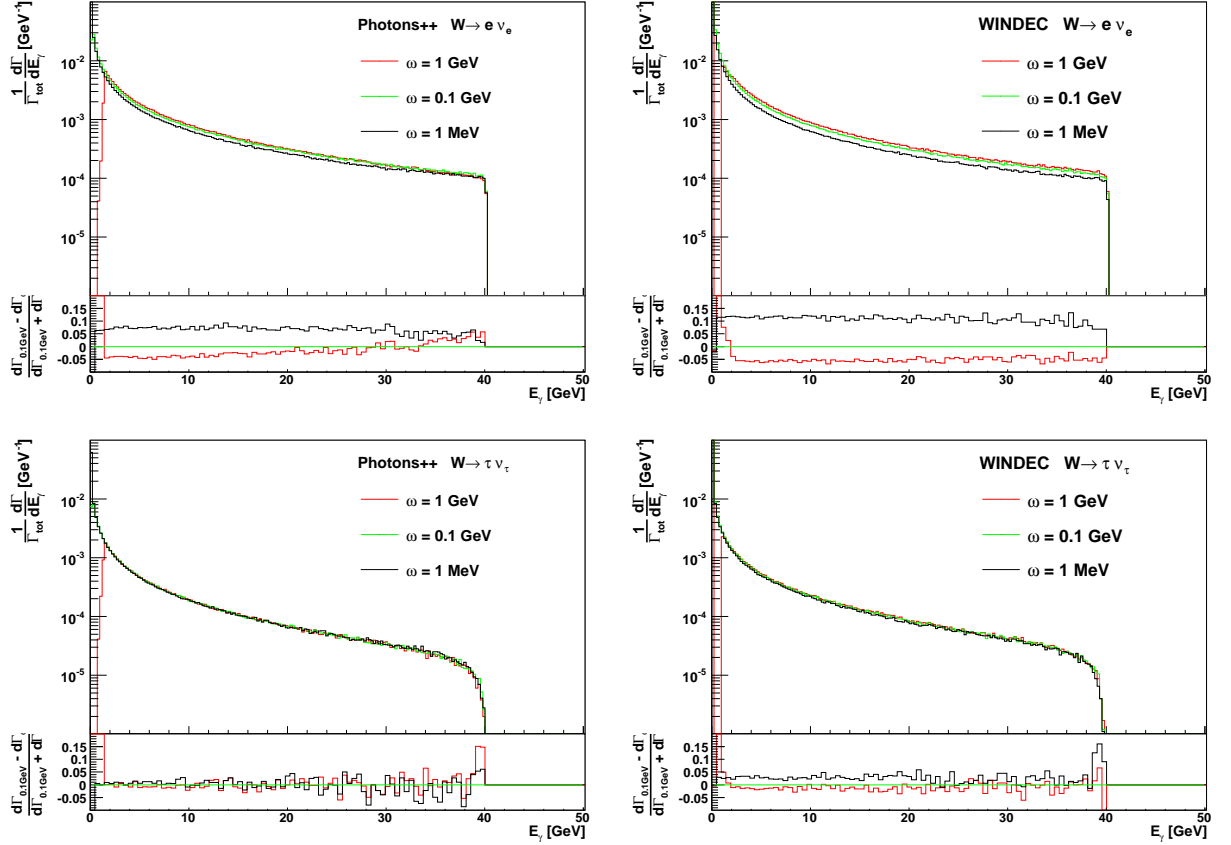


Figure 3: *Dependence of the total energy of the radiated photons' on the infrared cut-off in PHOTONS++ (left panel) and WINDEC (right panel) for $W \rightarrow e\nu_e$ (upper panel) and $W \rightarrow \tau\nu_\tau$ decays (lower panel). The relative difference to $\omega = 0.1\text{ GeV}$ is shown.*

has been neglected, which is strictly true only for $\omega \rightarrow 0$. Thus, some residual dependence is to be expected, even if infrared subtracted matrix element corrections were included to all orders. This dependence is of course minimised with small cut-offs.

5.1.3 Effects of inclusion of exact matrix elements

Including exact matrix elements, as discussed in Section 4.2, further improves the accuracy of the distributions. This is especially true away from the singular limits, where considerable differences emerge. This is exemplified in Fig. 6, where the angular distributions of photons in $Z \rightarrow \ell\bar{\ell}$ decays is depicted. Of course, there is also an effect on the differential decay rate. Fig. 6 shows that corrections obtained from the quasi-collinear approximation, i.e. from the approximate matrix element, overestimate the exact matrix element resulting in an increased differential decay rate. Even more so in the region of very hard photon emission which, due to the angular constraints imposed by the emitter's mass, no longer fulfils the condition $(p \cdot k) \rightarrow 0$.

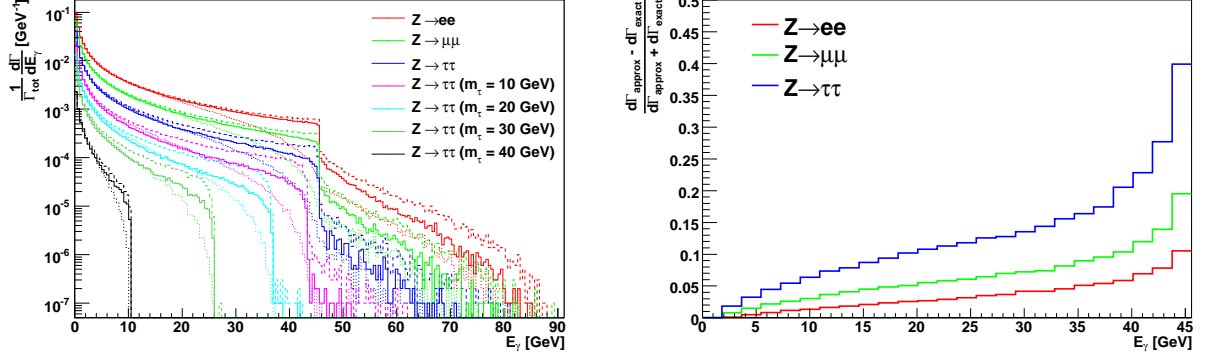


Figure 4: The total energy of all photons radiated in $Z \rightarrow \ell\bar{\ell}$. Left panel (a): The same plot as in Fig. 1(b), but this time the correction is done by using the **exact** matrix element (solid) instead of the **approximated** one (dashed). The distribution generated using the eikonals only is shown as a dotted line. Right panel (b): The relative difference of the distributions obtained using the exact and the approximated matrix elements. In both cases again different fermion masses have been used.

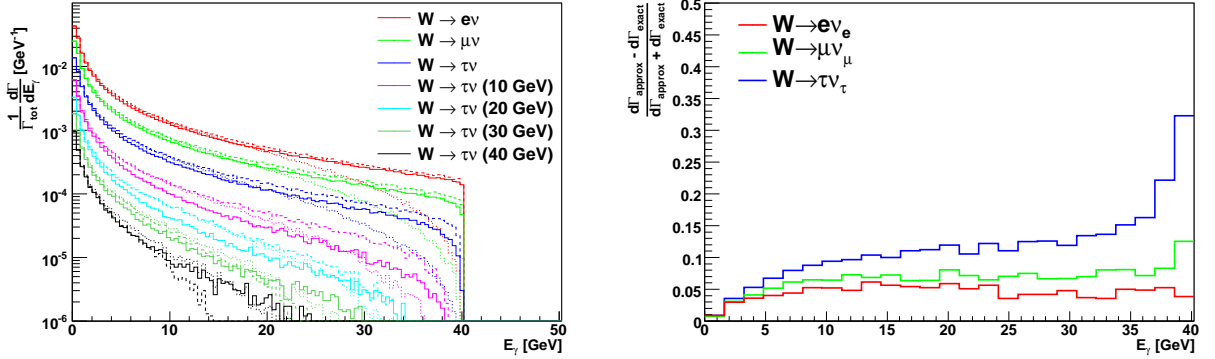


Figure 5: The total energy of all photons radiated in $W \rightarrow \ell\nu$. Left panel (a): The same plot as in Fig. 1(d), but this time the correction is done by using the **exact** matrix element (solid) instead of the **approximated** one (dashed). The distribution generated using the eikonals only is shown as a dotted line. Right panel (b): The relative difference of the distributions obtained using the exact and the approximated matrix elements. In both cases again different fermion masses have been used.

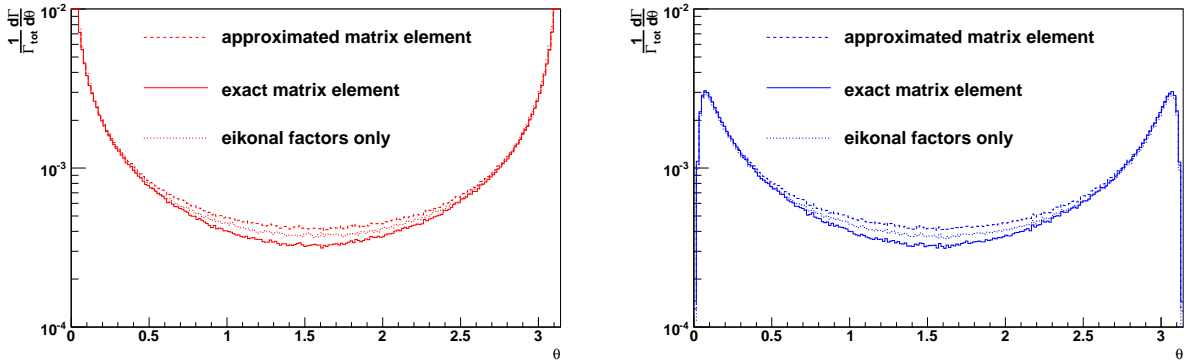


Figure 6: *Angular distributions of the emitted photons in $Z \rightarrow \ell\bar{\ell}$, using exact and approximated matrix elements. In the left panel (a) and the right panel (b), the cases $Z \rightarrow ee$ and $Z \rightarrow \tau\tau$ are exhibited using the eikonals only (dotted lines) and corrections through exact (solid) and approximated matrix elements (dashed). In both plots the leptons sit at $\theta = 0$ and $\theta = \pi$.*

Here the full matrix element exhibits some destructive interference between the two relevant diagrams which is of course absent in the treatment through the dipole splitting kernels. This leads to a slightly earlier drop-off of the differential decay rate w.r.t. radiated energy than with the approximated matrix elements.

Further, the absence of interference terms in both the eikonals and the quasi-collinear approximation leads to an overestimation of radiation at large angles. Because of only small correlations between the energy of the photon radiated and its angular distribution this overestimation leads to an almost constant decline in the differential decay rate w.r.t. the photon energy when corrected by the exact matrix element. Of course, while this effect is small in the decay channel $Z \rightarrow e^+e^-$, it increases with the mass of the emitter and when a larger fraction of the radiation is radiated at large angles. Nevertheless, for very high emitter masses (cf. the fictive τ with $m_\tau = 40\text{GeV}$ in Fig. 4) the approximation proves useful again. This is due to the dominance of the soft logarithms over the quasi-collinear ones in this limit.

5.2 Other channels

Finally, a short overview over other interesting cases is given. In principle, PHOTONS++ can handle any possible final state configuration in single particle decays independent of its charge. Thus, it is well suited to address all τ - and hadron decays, which will be the topic of this section.

5.2.1 J/Ψ decays to leptons

First of all, consider the case of $J/\Psi \rightarrow \ell\bar{\ell}$, which is topologically identical to leptonic Z -decay, but nonetheless very important for the calibration of detectors and as a background source of leptons. In Fig. 7 the decay channels $J/\psi \rightarrow e^+e^-$ and $J/\psi \rightarrow \mu^+\mu^-$ are investigated and the

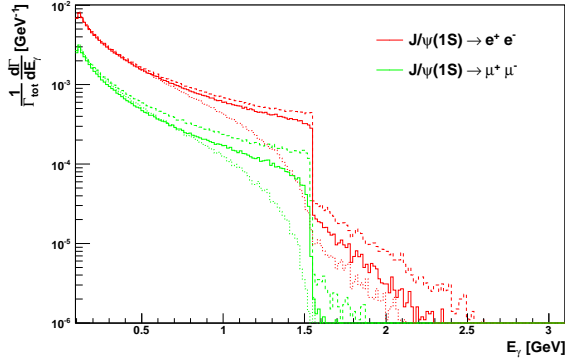


Figure 7: *The total energy of the radiated photons in the rest frame of the decaying J/ψ vector meson for different lepton pairs (electrons in red, muons in green) in the final state. $\mathcal{C} = 1$ (dotted) is contrasted with $\mathcal{C} = 1 + \tilde{\beta}_1^1/\tilde{\beta}_0^0$, where $\tilde{\beta}_1^1$ is calculated in the quasi-collinear approximation (dashed) and with the complete real emission matrix element (solid). In all cases, the distributions are normalised on the width of the inclusive decay into the respective lepton pair, and the infrared cut-off has been fixed to $\omega = 1\text{MeV}$.*

effect of $\mathcal{O}(\alpha)$ corrections is scrutinised. Again, the kinematic limit at half the mass of the decaying particle produces a visible and prominent kink. Due to the much smaller mass of the J/ψ compared to the Z mass, the effects of the higher muon mass are much more pronounced, both in the sharpness of the kink and the quality of the quasi-collinear approximation.

5.2.2 $B \rightarrow D^* +$ pions and semileptonic B decays

Another system to demonstrate the versatility of PHOTONS++ are B -decays because of its manifold topologies in the final state.

In Figure 8 semi-leptonic decays of B^0 mesons into D^- scalars and D^{*-} vectors are displayed. The resulting distributions are similar for e or μ being the lepton. This is because in both cases the bulk of the radiation is emitted off the lepton and the amount of phase space open for bremsstrahlung is of similar magnitude. Only the average photon multiplicity is noticeably affected by the difference in mass between the electron and the muon. The τ -channel on the other hand presents itself differently due to the mass of the tau being comparable both to the mass of the B^0 - and the $D^{(*)-}$ -mesons. This not only leads to the near absence of soft bremsstrahlung above the infrared cut-off, as compared to the other semi-leptonic channels, it also results in a completely different radiation pattern: The bulk of the photons is radiated in between both dipole particles and not primarily collinearly. Furthermore, the absence of interference terms in the radiation off the lepton-scalar pair in contrast to the lepton-vector pair is plainly visible for both e and μ . Again, the relevance of the interference terms is small for the τ -mode due to its radiation being dominated by the spin-independent soft terms. The exact matrix element correction also shows the shortcomings of the dipole splitting functions in this case as they fail to predict the excess of hard radiation for the electron. This attribute is

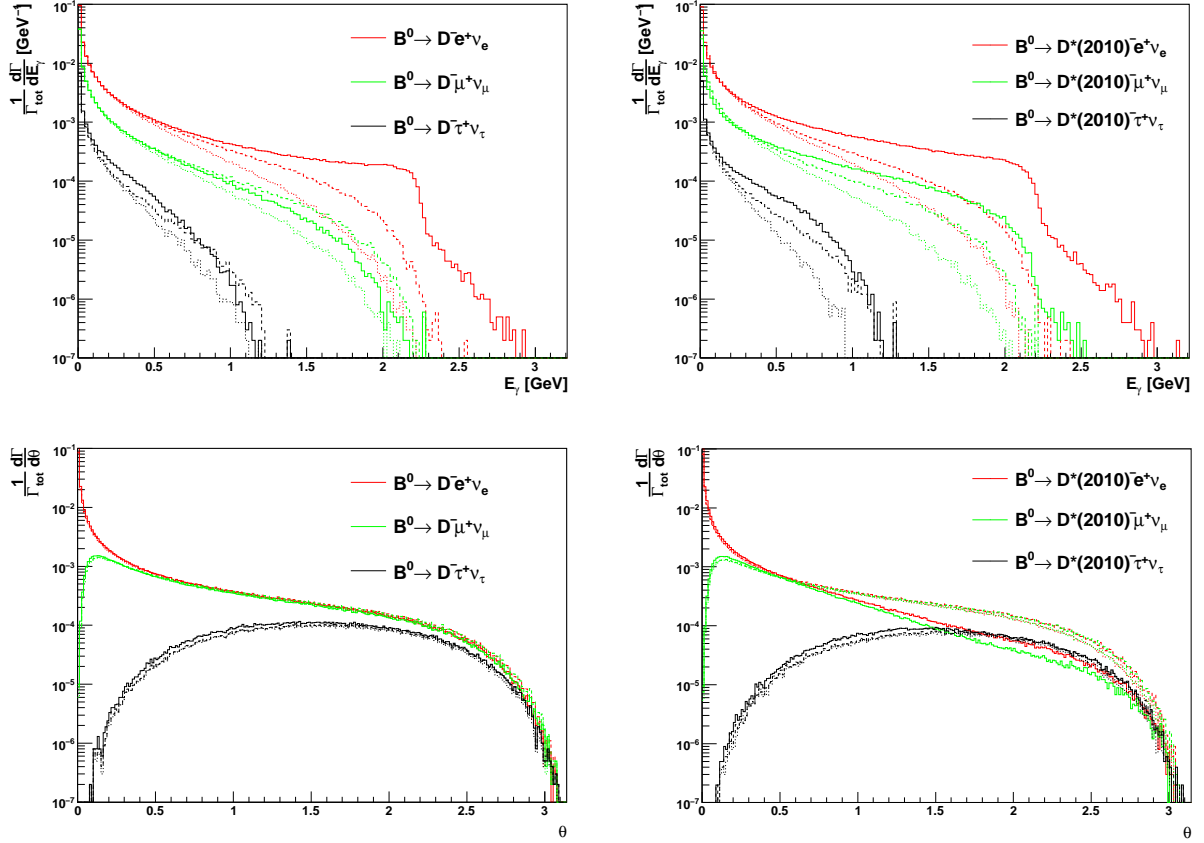


Figure 8: *Semi-leptonic decays $B^0 \rightarrow D^- \ell \nu$ and $B^0 \rightarrow D^{*(2010)-} \ell \nu$ for different leptons and with different matrix element corrections. The solid line corresponds to the correction using the full matrix elements in the point-like hadron approximation, the dashed line corresponds to the dipole splitting kernels neglecting interference terms and the dotted line corresponds to using the eikonals only. The angular distributions are shown in the $\ell - D^{(*)-}$ rest frame with the lepton at $\theta = 0$. Again, the infrared cut-off was set to 1MeV.*

shielded in the muon case by its already comparable large mass. However, the total radiative decay rate is nearly unaffected by this. The spin-dependence of the dipole approximation is also suppressed by the large mass of the D^- and D^{*-} , respectively, hence the small difference of both cases in that approximation.

As an example for dealing with multiple charged particles in the final state, B^0 decays into a D^* accompanied with various numbers of charged and neutral π 's have been chosen. The results are on display in Fig. 9, where the total radiated photon energy and the angular distribution of the photons are depicted. The orientation of the final state momenta has been chosen in such a way that configurations of the same multipole structure differing only by a neutral pion have a similar momentum distribution within the multipole, but still letting the π^0 have a non-vanishing effect. The most prominent feature in the distribution of the

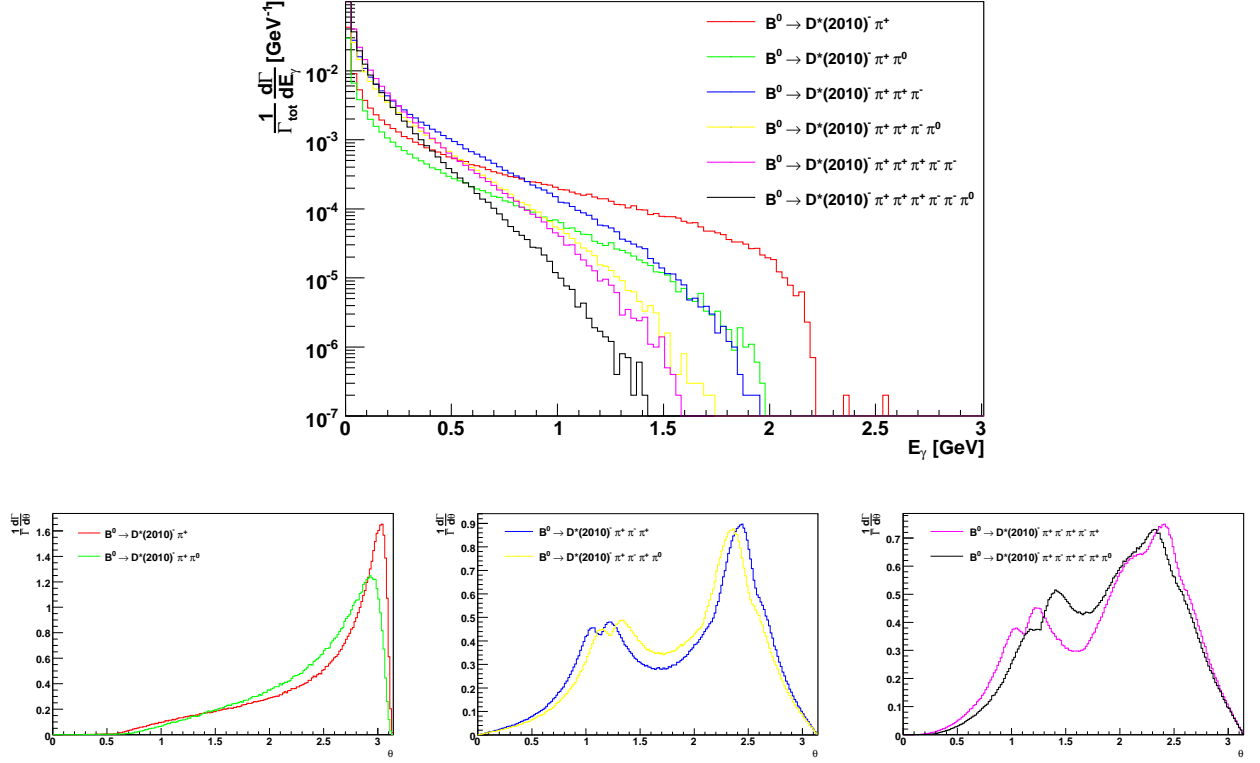


Figure 9: *The total photon energy in the rest frame of the decaying B^0 meson for different numbers of pions in the final state (upper plot) and the angular distribution of this radiation in the multipole rest frame with the D^{*-} at $\theta = 0$ (lower panel). For the multi-body final states the same kinematic configurations have been used, as detailed in the text, to yield easily interpretable results. For identical multipoles similar final state momentum configurations with non-vanishing π^0 momentum have been chosen to increase comparability. The infrared cut-off in all cases has been set to $\omega = 1\text{MeV}$.*

total energy of all photons in the B meson's rest frame is the receding kinematic limit for the total energy, it is independent of the momentum layout within the multipole. It is due to the decreasing amount of phase space open for bremsstrahlung with an increasing number of pions. On the other hand, while the total energy available for the photon decreases, the amount of Bremsstrahlung increases with the number of charged particles involved. Switching from a dipole (two charged particles) to a quadrupole (four charged particles), the probability of double hard photon emission is increased due to favourable momentum configurations among the strongly radiating pions. Additionally, since the pions are spin-0, their photon distribution is generated exclusively by a product of eikonal factors. Furthermore, the angular distributions of the emitted photons are shown. There, the differential cross-section is integrated over energy and the azimuthal angle. For better interpretability these distributions are plotted in the rest frame of the multipole. The $D^*(2010)^-$ always rests at $\theta = 0$. Due to its large mass, compared

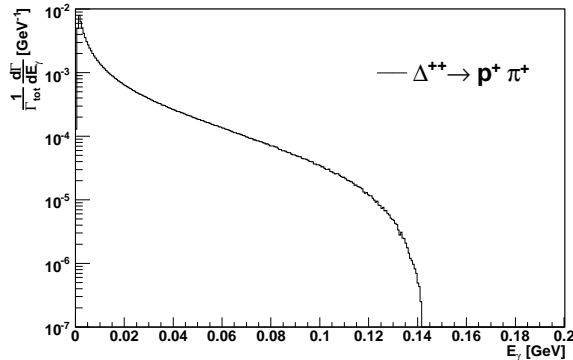


Figure 10: The total photon energy in $\Delta^{++} \rightarrow p^+ \pi^+$ in the rest frame of the decaying Δ^{++} baryon is exhibited. The infrared cut-off was set to 1keV.

to the pions, very little radiation is emitted in its direction. In contrast, all charged pions are plainly visible as peaks in the spectrum. However, their respective mass cones are hidden due to the azimuthal integration unless the pion sits at $\theta = \pi$, as is the case in the dipole configurations.

5.2.3 $\Delta^{++} \rightarrow p^+ \pi^+$ decays

A rather exotic decay for the purpose of this publication is the decay $\Delta^{++} \rightarrow p^+ \pi^+$, due to its lack of neutral particles. This case is presented in Fig. 10, where the total energy and the angular distribution of the emitted photons are exhibited. However, this channel leaves only very little phase space open for photon radiation. Thus, collinear enhancement for the p^+ and the Δ^{++} should be negligible.

5.2.4 τ decays

The leptonic τ decays are an example of a final state containing multiple neutral and massless particles. This has the effect that the leading order decays do not have a fixed momentum distribution among the primary decay products leading to a smearing out of the sharp kink at $\frac{1}{2}m_\tau$, as depicted in Figure 11. Because of the relatively small τ -mass and the considerable fraction of momentum carried by the neutrinos the effects of the different masses of the electron and the muon are plainly visible, in the photon energy spectrum as well as the angular distribution.

Furthermore, the branching fraction of radiative leptonic decays in μ and τ decays (with at least one photon with $E_\gamma > 10\text{MeV}$) has been checked against PDG values [25], cf. Tab. 2.

6 Conclusions and outlook

In this publication a new implementation of the YFS approach to the description of higher-order QED corrections in particle processes has been presented in the form of a Monte Carlo

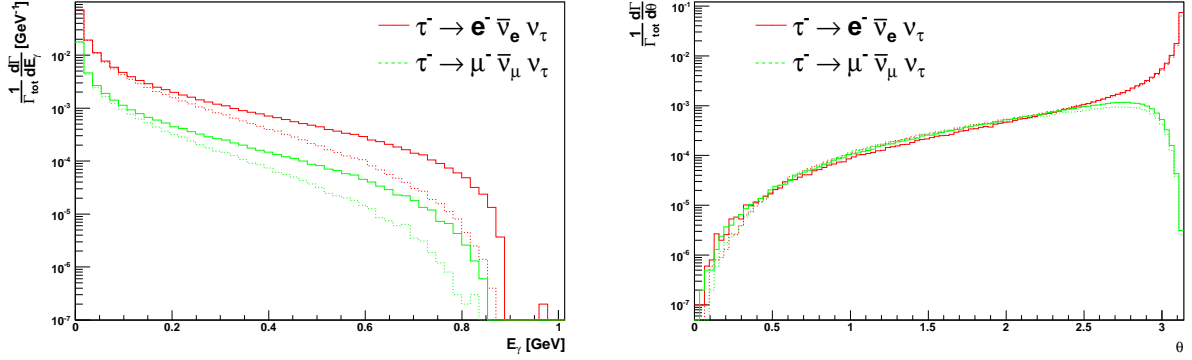


Figure 11: The total photon energy in $\tau^- \rightarrow \ell^- \bar{\nu}_\ell \nu_\tau$ in the rest frame of the decaying τ lepton is shown in the left panel. In the right panel the distribution of the photons' polar angle is shown in the $\tau - \ell$ rest frame with the τ at $\theta = 0$. In both plots, the solid line shows the distribution corrected with the exact matrix element and the dotted line the one using the eikonals only. The infrared cut-off was set to 1MeV .

	$\frac{\Gamma(\mu \rightarrow e \nu_e \nu_\mu \gamma)}{\Gamma(\mu \rightarrow e \nu_e \nu_\mu, \text{incl.})}$	$\frac{\Gamma(\tau \rightarrow e \nu_e \nu_\tau \gamma)}{\Gamma(\tau \rightarrow e \nu_e \nu_\tau, \text{incl.})}$	$\frac{\Gamma(\tau \rightarrow \mu \nu_\mu \nu_\tau \gamma)}{\Gamma(\tau \rightarrow \mu \nu_\mu \nu_\tau, \text{incl.})}$
PDG	0.014(4)	0.09(1)	0.021(3)
PHOTONS++	0.0147(1)	0.0999(3)	0.0233(2)

Table 2: A comparison of the branching ratios of the radiative leptonic μ and τ decay mode ($E_\gamma > 10\text{MeV}$) in relation to their inclusive leptonic mode calculated by PHOTONS++ and the PDG world average. The number in brackets reflects the absolute error on the last digit.

code. It is a part of the multi-purpose event generation framework SHERPA since version 1.1 and allows for a simulation of photon radiation in particle decays. This is an important effect with important experimental consequences. The huge advantage of the YFS approach is that it can be systematically improved order-by-order in the electromagnetic coupling constant, such that its accuracy can be increased to match exact results at in principle any given perturbative order. Thus, in terms of possible accuracy, the YFS approach clearly reaches beyond typical parton-shower based algorithms. Some of the effects due the inclusion of exact perturbative results have been studied in this publication.

In contrast to another recent implementation of the YFS approach in SOPHTY, here, in PHOTONS++, there is no constraint in the number of particles produced in the decay, i.e. PHOTONS++ stretches beyond the level of $1 \rightarrow 2$ decays. This is possible due to a new method of reconstructing the kinematics after QED radiation has been added to a core process, thus shifting its characteristics *a posteriori*. The corresponding algorithms have been tested and validated in detail through comparison with results from other codes and experimental data. Some of the results have also been presented in this paper.

It is anticipated that in the progress of the further development of SHERPA also its modules will be improved; in the case of PHOTONS++ this will mainly involve the addition of an increasing number of exact higher order results. Some of the most relevant $1 \rightarrow 2$, such as generic $V \rightarrow FF$ matrix elements with adjustable couplings, cf. Sec. 4.1, $S \rightarrow FF$ and $S \rightarrow SS$, as well as more dedicated $W \rightarrow \ell\nu$, $\tau \rightarrow \ell\nu_\ell\nu_\tau$, $S \rightarrow S\ell\nu$ and $S \rightarrow V\ell\nu$ are already present. Others will need to be added. The structure of the code also permits the inclusion of form-factors to take into account the composite nature of hadrons.

Acknowledgements

The authors wish to thank K. Hamilton, S. Jadach, P. Richardson and Z. Was for fruitful discussions and C. M. Carloni Calame for help with the correct usage of HORACE. M.S. wishes to thank the INP for a pleasant atmosphere and great support during the initial stages of this project. M.S. would also like to thank D. Stöckinger for many fruitful discussions. Financial support by MCnet (contract number MRTN-CT-2006-035606), DAAD and BMBF is gratefully acknowledged. M.S. wishes to thank the DAAD for financial support for the scientific visit to INP Cracow.

A The YFS-Form-Factor

In this appendix, the cancellation of virtual and real soft singularities will explicitly be performed and the YFS-Form-Factor will be calculated. As already defined in Sections 2 and 3 the YFS-Form-Factor $Y(\Omega)$ reads

$$Y(\Omega) = 2\alpha \sum_{i < j} \left(\mathcal{R}e B(p_i, p_j) + \tilde{B}(p_i, p_j, \Omega) \right),$$

where the virtual infrared factor is given by

$$B(p_i, p_j) = -\frac{i}{8\pi^3} Z_i Z_j \theta_i \theta_j \int \frac{d^4 k}{k^2} \left(\frac{2p_i \theta_i - k}{k^2 - 2(k \cdot p_i) \theta_i} + \frac{2p_j \theta_j + k}{k^2 + 2(k \cdot p_j) \theta_j} \right)^2$$

and the real infrared factor reads

$$\tilde{B}(p_i, p_j, \Omega) = \frac{1}{4\pi^2} Z_i Z_j \theta_i \theta_j \int d^4 k \delta(k^2) (1 - \Theta(k, \Omega)) \left(\frac{p_i}{(p_i \cdot k)} - \frac{p_j}{(p_j \cdot k)} \right)^2.$$

As before, Z_i and Z_j are the charges of particles i and j in units of the positron charge, respectively, and the sign factors $\theta_{i,j} = \pm 1$ for final (initial) state particles. Again, Ω is the “unresolved” region of the phase space for the soft photons. In this form the divergences need to be regularised, which can be achieved by either introducing a fictitious small photon mass λ , as in the original YFS paper [8], or through dimensional regularisation. In both cases, however, the limited real emission phase space Ω will lead to potentially large logarithms.

After performing the momentum integration, the virtual infrared factor can be written as

$$B(p_i, p_j) = -\frac{Z_i Z_j \theta_i \theta_j}{2\pi} \left(\ln \frac{m_i m_j}{\lambda^2} + \frac{1}{2} (p_i \cdot p_j) \theta_i \theta_j \int_{-1}^1 dx \frac{\ln \frac{p_x'^2}{\lambda^2}}{p_x'^2} + \frac{1}{4} \int_{-1}^1 dx \ln \frac{p_x'^2}{m_i m_j} \right),$$

where

$$p_x' = \frac{(p_i \theta_i - p_j \theta_j) + x(p_i \theta_i + p_j \theta_j)}{2}$$

and

$$-\ln \lambda^2 = \frac{1}{\epsilon} - \ln \tilde{\mu}^2$$

contains the infrared divergence. Similarly, the real infrared factor reads

$$\begin{aligned} \tilde{B}(p_i, p_j, \omega) = & \frac{Z_i Z_j \theta_i \theta_j}{2\pi} \left[\ln \frac{\omega^2}{\lambda^2} + \ln \frac{m_i m_j}{E_i E_j} - \frac{1}{2} (p_i \cdot p_j) \int_{-1}^1 dx \frac{\ln \frac{p_x'^2}{\lambda^2}}{p_x'^2} + \frac{1}{2} (p_i \cdot p_j) \int_{-1}^1 dx \frac{\ln \frac{E_x^2}{\omega^2}}{p_x^2} \right. \\ & \left. - \tilde{G}(1) - \tilde{G}(-1) + (p_1 \cdot p_2) \int_{-1}^1 dx \frac{\tilde{G}(x)}{p_x^2} \right], \end{aligned}$$

with

$$p_x = \frac{(p_i + p_j) + x(p_i - p_j)}{2}$$

and ω is the momentum cut-off specifying Ω in the frame \tilde{B} is to be evaluated in. Furthermore,

$$\tilde{G}(x) = \frac{1 - \beta_x}{2\beta_x} \ln \frac{1 + \beta_x}{1 - \beta_x} + \ln \frac{1 + \beta_x}{2}.$$

with

$$\beta_x = \frac{|\vec{p}_x|}{p_x^0} = \frac{\sqrt{(\vec{p}_i + \vec{p}_j)^2 + 2x(\vec{p}_i^2 - \vec{p}_j^2) + x^2(\vec{p}_i - \vec{p}_j)^2}}{(E_i + E_j) + x(E_i - E_j)}.$$

Combining both terms to the YFS-Form-Factor the divergences cancel and a finite result is obtained. The remaining parameter integrals do not give rise to further divergences as long as $p_i^2, p_j^2 > 0$, i.e. as long as the emitting particles are massive. Thus, taken together, the YFS form factor reads

$$\begin{aligned} Y(p_i, p_j, \omega) = & -\frac{\alpha}{\pi} Z_i Z_j \theta_i \theta_j \left[\ln \frac{E_i E_j}{\omega^2} - \frac{1}{2} (p_i \cdot p_j) \int_{-1}^1 dx \frac{\ln \frac{E_x^2}{\omega^2}}{p_x^2} + \frac{1}{4} \int_{-1}^1 dx \ln \frac{p_x'^2}{m_i m_j} \right. \\ & + \frac{1}{2} (p_i \cdot p_j) \Theta(\theta_i \theta_j) \left(\frac{8\pi^2 \Theta(x'_1 x'_2)}{(x'_2 - x'_1)(p_i + p_j)^2} + \int_{-1}^1 dx \frac{\ln x^2}{p_x^2} \right) \\ & \left. + \tilde{G}(1) + \tilde{G}(-1) - (p_i \cdot p_j) \int_{-1}^1 dx \frac{\tilde{G}(x)}{p_x^2} \right], \end{aligned}$$

where $x'_{1,2}$ are the roots of $p_x'^2$ with $x'_1 < x'_2$. The general case cannot be evaluated in closed form. This is due to the fact that the term

$$\int_{-1}^1 dx \frac{\tilde{G}(x)}{p_x^2},$$

although completely finite, can only be evaluated analytically for the dipole in its rest frame or in the rest frame of one of either of its constituent particles. This can only be achieved if there is one dipole only. All other cases need to be evaluated numerically.

A.1 Special cases

A.1.1 Decay into two particles with $(p_i \theta_i + p_j \theta_j)^2 < 0$

If the multipole consists of only two particles in the final state, e.g. for decays of the type $Z \rightarrow \ell\ell$, then there is an analytical solution in the rest frame of the dipole formed by the two

charged particles. In the high-energy limit, given by $E_i \gg m_i$ for both QED corrected charged particles, the critical term above can be written as

$$(p_i \cdot p_j) \int_{-1}^1 dx \frac{\tilde{G}(x)}{p_x^2} \cong \frac{1}{6} \pi^2.$$

Therefore, in this case, the full YFS form factor reads

$$Y(p_i, p_j, \omega) \cong -\frac{\alpha}{\pi} Z_i Z_j \theta_i \theta_j \left[\left(1 - \ln \frac{2(p_i \cdot p_j)}{m_i m_j} \right) \ln \frac{E_i E_j}{\omega^2} + \ln \frac{E_i}{E_j} \ln \frac{m_i}{m_j} - \frac{1}{2} \ln^2 \frac{E_i}{E_j} + \frac{1}{2} \ln \frac{(p_i \theta_i + p_j \theta_j)^2}{m_i m_j} - 1 - \frac{\pi^2}{6} \right].$$

This result in the high-energy limit agrees with the result stated in [8].

A.1.2 Decay of a charged particle with one charged final state with $(p_i \theta_i + p_j \theta_j)^2 = 0$

A similar, but nonetheless different case occurs for the decay of a charged particle into a final state involving only one charged particle, e.g. the case of W -decays, $W \rightarrow \ell \nu_\ell$. Then, in the corresponding dipole's rest frame neither $m_W \ll E_W$ nor $(p_i \theta_i + p_j \theta_j)^2 < 0$ and therefore this case is different from the one above. In this case, for $(p_W - p_l)^2 = 0$,

$$Y_W(\omega) = \frac{\alpha}{\pi} \left[2 \left(1 - \ln \frac{m_W}{m_l} \right) \ln \frac{m_W}{\omega \sqrt{8}} + \ln \frac{m_W}{m_l} - \frac{1}{2} + \frac{3}{2} \ln 2 - \frac{3}{12} \pi^2 \right].$$

This result of course differs from the result in [24] since both results are given in different Lorentz-frames. Also, if in this process a photon is radiated, then $(p_W - p_l)^2 = 2(p_\nu \cdot p_\gamma) > 0$ and the YFS-Form-Factor takes a different a form.

A.2 The full YFS form factor

Here the complete solutions to analytically integrable parameter integrals in the YFS form factor are given. In the following, using the invariance of $Y(\Omega)$ under the interchange of $p_i \leftrightarrow p_j$, the labels p_i and p_j are chosen such that $E_j \geq E_i$. It is useful to define

$$x_{1,2} = - \frac{p_i^2 - p_j^2 \pm 2\sqrt{(p_i \cdot p_j)^2 - p_i^2 p_j^2}}{(p_i - p_j)^2}$$

as the roots of p_x^2 and

$$x'_{1,2} = - \frac{p_i^2 - p_j^2 \pm 2\sqrt{(p_i \cdot p_j)^2 - p_i^2 p_j^2}}{(p_i + p_j)^2}$$

as those of $p_x'^2$ in case of $\theta_i\theta_j = +1$, satisfying $x_{1,2} \notin [-1, 1]$ and $x'_{1,2} \in (-1, 1)$, respectively. It holds that $x_1, x'_2 > 0$ and $x_2, x'_1 < 0$ if $(p_i - p_j)^2 < 0$ and $0 < x_1 < x_2$ and $0 < x'_1 < x'_2$ if $(p_i - p_j)^2 > 0$. These difference in the relations between x_1 and x_2 necessitate the differentiation of distinct cases in the calculations.

If $(p_i - p_j)^2 = 0$ then $x_{1,2}$ are not defined. If $\theta_i\theta_j = -1$ then $p_x'^2 = p_x^2$ and $x'_{1,2}$ are meaningless, leading to another set of distinct cases.

When evaluating the first set of the parameter integrals that fact simplifies matters a lot resulting in

$$\mathcal{R}e \left(\theta_i\theta_j \int_{-1}^1 dx \frac{\ln \frac{p_x'^2}{\lambda^2}}{p_x'^2} + \int_{-1}^1 dx \frac{\ln \frac{p_x^2}{\lambda^2}}{p_x^2} \right) \stackrel{\theta_i\theta_j=-1}{=} 0.$$

Otherwise, the evaluation is more complicated and involves shifting the poles at $x'_{1,2}$ off the real axis. The solution then is

$$\begin{aligned} \mathcal{R}e \left(\theta_i\theta_j \int_{-1}^1 dx \frac{\ln \frac{p_x'^2}{\lambda^2}}{p_x'^2} + \int_{-1}^1 dx \frac{\ln \frac{p_x^2}{\lambda^2}}{p_x^2} \right) \\ = \frac{8\pi^2\Theta(x'_1x'_2)}{(x'_2 - x'_1)(p_i + p_j)^2} + \frac{8}{(x_1 - x_2)(p_i - p_j)^2} \left[\ln |x_1| \left(\text{Li}_2 \left(\frac{x_1-1}{x_1} \right) - \text{Li}_2 \left(\frac{x_1+1}{x_1} \right) \right) \right. \\ \left. - \ln |x_2| \left(\text{Li}_2 \left(\frac{x_2-1}{x_2} \right) - \text{Li}_2 \left(\frac{x_2+1}{x_2} \right) \right) \right]. \end{aligned}$$

In any case, the last piece of the divergence has cancelled, leaving finite terms negligible in the high energy limit.

The other integral containing $p_x'^2$ is to be evaluated next. In total there are three cases to consider.

- $\theta_i\theta_j = +1$

$$\begin{aligned} \mathcal{R}e \left(\int_{-1}^1 dx \ln \frac{p_x'^2}{m_i m_j} \right) \\ = 2 \ln \frac{(p_i + p_j)^2}{4m_i m_j} + \ln [(1 - x_1'^2)(1 - x_2'^2)] - x'_1 \ln \left| \frac{1 - x'_1}{1 + x'_1} \right| - x'_2 \ln \left| \frac{1 - x'_2}{1 + x'_2} \right| - 4. \end{aligned}$$

Although, there again are poles within the range of integration the integral over them is finite.

- $\theta_i\theta_j = -1$. The range of integration does not comprise any poles and, thus, is real, giving

$$\begin{aligned} \int_{-1}^1 dx \ln \frac{p_x^2}{m_i m_j} \\ = 2 \ln \frac{|(p_i - p_j)^2|}{4m_i m_j} + \ln [(1 - x_1^2)(1 - x_2^2)] + x_1 \ln \left| \frac{1 + x_1}{1 - x_1} \right| + x_2 \ln \left| \frac{1 + x_2}{1 - x_2} \right| - 4. \end{aligned}$$

Evidently, the case $(p_i - p_j)^2 = 0$ has to be treated separately. It yields

$$\int_{-1}^1 dx \ln \frac{p_x^2}{m_i m_j} = 2 \ln \frac{|p_i^2 - p_j^2|}{2m_i m_j} + \ln |1 - x_p^2| + x_p \ln \left| \frac{1 + x_p}{1 - x_p} \right| - 2.$$

where $x_p = -\frac{p_i^2 + p_j^2}{p_i^2 - p_j^2}$. In decay matrix elements it is not kinematically possible to also have $m_i = m_j$.

The last integral that is generally solveable analytically differentiates even more cases. The easiest to solve is the case of $E_i = E_j$, as it is occurring in leptonic Z -decays. Here, E_x is independent of x , thus giving

$$\int_{-1}^1 dx \frac{\ln \frac{E_x^2}{\omega^2}}{p_x^2} = \frac{8}{(x_1 - x_2)(p_i - p_j)^2} \ln \frac{E_i + E_j}{2\omega} \ln \left| \frac{(1 - x_1)(1 + x_2)}{(1 + x_1)(1 - x_2)} \right|.$$

For all other dipoles three distinct cases appear:

- $(p_i - p_j)^2 < 0$

$$\begin{aligned} & \int_{-1}^1 dx \frac{\ln \frac{E_x^2}{\omega^2}}{p_x^2} \\ &= \frac{8}{(x_1 - x_2)(p_i - p_j)^2} \left[\ln \frac{E_i}{\omega} \ln \left| \frac{1 - x_1}{1 + x_1} \right| + \ln |y_1| \ln \left| \frac{1 - x_1}{1 + x_1} \right| \right. \\ & \quad - \ln \frac{(1 + x_2)E_i + (1 - x_2)E_j}{2\omega} \ln \left| \frac{1 - x_2}{1 + x_2} \right| \\ & \quad \left. + \text{Li}_2 \left(-\frac{\zeta(1+x_1)}{y_1} \right) - \text{Li}_2 \left(\frac{\zeta(1-x_1)}{y_1} \right) - \text{Li}_2 \left(-\frac{1+x_2}{x_E - x_2} \right) + \text{Li}_2 \left(\frac{1-x_2}{x_E - x_2} \right) \right] \end{aligned}$$

with $y_1 = 1 + \zeta(1 - x_1)$, $\zeta = -\frac{E_i - E_j}{2E_i}$ and $x_E = -\frac{E_i + E_j}{E_i - E_j}$.

- $(p_i - p_j)^2 > 0$

$$\begin{aligned}
& \int_{-1}^1 dx \frac{\ln \frac{E_i^2}{\omega^2}}{p_x^2} \\
&= \frac{8}{(x_1 - x_2)(p_i - p_j)^2} \left[\ln \frac{E_i}{\omega} \ln \left| \frac{1 - x_1}{1 + x_1} \right| + \ln |y_1| \ln \left| \frac{1 - x_1}{1 + x_1} \right| \right. \\
&\quad + \frac{1}{2} \ln^2 \left| \frac{y_2}{\xi(1 + x_2)} \right| - \frac{1}{2} \ln^2 \left| \frac{y_2}{\xi(1 - x_2)} \right| \\
&\quad - \ln \frac{E_j}{\omega} \ln \left| \frac{1 - x_2}{1 + x_2} \right| + \ln |y_2| \ln \left| \frac{1 - x_2}{1 + x_2} \right| \\
&\quad \left. + \text{Li}_2 \left(-\frac{\xi(1+x_1)}{y_1} \right) - \text{Li}_2 \left(\frac{\xi(1-x_1)}{y_1} \right) - \text{Li}_2 \left(-\frac{y_2}{\xi(1-x_2)} \right) + \text{Li}_2 \left(\frac{y_2}{\xi(1+x_2)} \right) \right]
\end{aligned}$$

with $y_2 = 1 + \xi(1 + x_2)$ and $\xi = \frac{E_i - E_j}{2E_j}$.

- $(p_i - p_j)^2 = 0$

With the definitions for x_E and x_p from above it always holds that $x_E > x_p > 1$, thus

$$\begin{aligned}
& \int_{-1}^1 dx \frac{\ln \frac{E_i^2}{\omega^2}}{p_x^2} \\
&= \frac{4}{p_j^2 - p_i^2} \left[\ln \frac{E_j - E_i}{2\omega} \ln \left| \frac{1 + x_p}{1 - x_p} \right| + \ln(x_E - x_p) \ln \left| \frac{1 + x_p}{1 - x_p} \right| \right. \\
&\quad \left. + \text{Li}_2 \left(\frac{x_p - 1}{x_p - x_E} \right) - \text{Li}_2 \left(\frac{x_p + 1}{x_p - x_E} \right) \right]
\end{aligned}$$

The last integral can generally only be solved numerically. This is due to the complexity of β_x . If, however, the dipole is in its rest frame or in the rest frame of one of its constituents, there are analytical solutions. Because PHOTONS++ always treats multipoles in their rest frames solutions for the integral will only be given in that frame. Two important cases are:

- $m_i = m_j$

$$\begin{aligned}
& \int_{-1}^1 dx \frac{\tilde{G}(x)}{p_x^2} \\
&= \frac{1}{\beta E^2} \left[\frac{1}{2} \ln^2 \frac{1 + \beta}{2} + \ln 2 \ln(1 + \beta) - \frac{1}{2} \ln^2 2 - \frac{1}{2} \ln^2(1 + \beta) \right. \\
&\quad \left. + \text{Li}_2 \left(\frac{1 - \beta}{2} \right) - \text{Li}_2 \left(\frac{1 + \beta}{2} \right) + \text{Li}_2(\beta) - \text{Li}_2(-\beta) \right]
\end{aligned}$$

with $\beta = \frac{|\vec{p}_i|}{E_i} = \frac{|\vec{p}_j|}{E_j}$ and $E = E_i = E_j$.

- Leptonic W -decay ($m_i \ll m_j = m_W$)

$$\int_{-1}^1 dx \frac{\tilde{G}(x)}{p_x^2} \cong \frac{2}{m_j^2} \left[\frac{3}{12} \pi^2 + \text{Li}_2(-2) \right].$$

B Transforming the phase space elements

This section details the phase space manipulations necessary for the implementation of the YFS algorithm in form of a computer code.

B.1 Rewriting the phase space element in other frames

As discussed in Sec. 3.2, the phase space integral with the phase space element

$$\begin{aligned} d\Phi &= d\Phi_p d\Phi_k (2\pi)^4 \delta(p_C + p_N - P_C - P_N - K) \\ &= \prod_{i=1}^n \left[\frac{d^3 p_i}{(2\pi)^3 2p_i^0} \right] \prod_{i=1}^{n_\gamma} \left[\frac{d^3 k}{k^0} \right] (2\pi)^4 \delta(p_C + p_N - P_C - P_N - K), \end{aligned}$$

has to be transformed to explicitly be in the chosen frame, the multipole rest frame. This can be achieved by using the identities

$$\begin{aligned} 1 &= \frac{2}{M^2} \int d^4(p_C + p_N) d^4 P_C dm_{M,p}^2 \delta\left(\frac{1}{M}(\vec{p}_C + \vec{p}_N)\right) \delta((p_C + p_N)^2 - M^2) \\ &\quad \times \delta^4\left(P_C + P_N - \sum p_i\right) \delta((p_C + P_C)^2 - m_{M,p}^2) \Theta((p_C + p_N)^0). \end{aligned}$$

and

$$1 = \frac{2}{m_{M,p}^4} \int d^4 x \delta\left(\frac{x^2}{m_{M,p}^2} - 1\right) \delta^3\left(\frac{1}{m_{M,p}} L^{-1}(p_C + P_C)\right). \quad (78)$$

Here, $m_{M,p}$ is the invariant mass of $P_M = p_C + P_C$ and M is the invariant mass of the initial state $p_C + p_N$. As before, p_C and p_N and P_C and P_N are the sums of the initial and final state charged and neutral particles' momenta. The first identity basically amounts to extending the integration to an integration over the full phase space including the initial particles. The second identity, taken from [26], involves a Lorentz-transformation, denoted by L^{-1} , being the boost into the rest frame of x . Applying this boost on the phase space integral of course is a valid operation, since the full expression at this point is formulated in a Lorentz-invariant way. The

result of this Lorentz-transformation, after inserting both identities, reads

$$\begin{aligned}
d\Phi &= (2\pi)^4 d\Phi_p d\Phi_k \int d^4(p_C + p_N) d^4 P_C dm_{M,p}^2 d^4 x \frac{2}{M^2} \frac{2}{m_{M,p}^4} \delta^4(p_C + p_N - P_C - P_N - K) \\
&\quad \times \delta^3(L(p_C + p_N)) \delta((p_C + p_N)^2 - M^2) \delta^4\left(P_C + P_N - \sum p_i\right) \\
&\quad \times \delta((p_C + P_C)^2 - m_{M,p}^2) \Theta((p_C + p_N)^0) \\
&\quad \times \delta\left(\frac{x^2}{m_{M,p}^2} - 1\right) \delta^3\left(\frac{1}{m_{M,p}}(\vec{p}_C + \vec{P}_C)\right).
\end{aligned}$$

Reordering and using the identity

$$\delta\left(\frac{x^2}{m_{M,p}^2} - 1\right) = \int dM^2 \delta\left(\frac{x^2}{M^2} - 1\right) \delta(M^2 - m_{M,p}^2)$$

yields

$$\begin{aligned}
d\Phi &= (2\pi)^4 d\Phi_p d\Phi_k \int d^4(p_C + p_N) d^4 P_C dm_{M,p}^2 \frac{2}{M^2} \frac{2}{m_{M,p}} \delta((p_C + p_N)^2 - M^2) \\
&\quad \times \delta^3(\vec{p}_C + \vec{P}_C) \delta^4(p_C + p_N - P_C - P_N - K) \delta^4\left(P_C + P_N - \sum p_i\right) \\
&\quad \times \delta((p_C + P_C)^2 - m_{M,p}^2) \Theta((p_C + p_N)^0) \\
&\quad \times \int d^4 x dM^2 \delta\left(\frac{x^2}{m_{M,p}^2} - 1\right) \delta^3\left(\frac{1}{M} L(p_C + p_N)\right) \delta(M^2 - m_{M,p}^2).
\end{aligned}$$

The last line can be further simplified by using the identity of Eq. (78) again and by integrating over M^2 . Now, the other integrations can be performed, first over $(p + p_N)$, then over P and finally over $m_{M,p}^2$. This results in

$$d\Phi = (2\pi)^4 d\Phi_p d\Phi_k \frac{2m_{M,p}^3}{M^2} \delta^3\left(2 \sum \vec{p}_i - \vec{P}_N + \vec{K} - \vec{p}_N\right) \delta\left(\left(\sum p_i + K\right)^2 - M^2\right),$$

where $m_{M,p}^2 = (p_C + P_C)^2 = (2 \sum p_i - P_N + K - p_N)^2 = P_M^2$ is the invariant mass of the QED-corrected multipole.

Finally, the identity

$$\delta\left(\left(\sum p_i + K\right)^2 - M^2\right) = \frac{1}{2(P_C^0 + P_N^0 + K^0)} \delta(P_M^0 - P_{M,0}^0)$$

will be used, where $P_{M,0}^0 = P_C^0 + p_C^0 = m_{M,p}$ and where all zero-components are taken in the rest frame of $P_M = p_C + P_C$. Therefore,

$$d\Phi = (2\pi)^4 \frac{m_{M,p}^3}{M^2(P_C^0 + P_N^0 + K^0)} d\Phi_p d\Phi_k \delta^3(\vec{P}_M) \delta(P_M^0 - P_C^0 - p_C^0).$$

The phase space element $d\Phi$ has thus been explicitly rewritten in the rest frame of the multipole, at the cost of a Jacobian.

Similarly, the zeroth order uncorrected cross section can be transformed to

$$\begin{aligned} d\Phi_0 &= (2\pi)^4 d\Phi_q \delta^4(p_C + p_N - Q_C - Q_N) \\ &= (2\pi)^4 \frac{m_{M,q}^3}{M^2(Q_C^0 + Q_N^0)} d\Phi_q \delta^3(\vec{Q}_M) \delta(Q_M^0 - Q_C^0 - p_C^0). \end{aligned}$$

where $m_{M,q}$ is the invariant mass of the uncorrected multipole and the Q_C^0 and Q_N^0 are taken in the Q_M rest frame.

B.2 Rewriting the phase space element in terms of the undressed momenta

In both cases the manipulations can be done in close analogy to the unitary algorithm of [27]. The necessary manipulations are easiest done backwards, starting with the phase space integral in terms of the q_i and defining $n = n_C + n_N$ to be the number of final state particles.

B.2.1 Mixed multipoles

In this case the starting point reads

$$\begin{aligned} &\int \prod_{i=1}^n \frac{d^3 q_i}{2q_i^0} \delta^3(Q_M^0) \delta(Q_M^0 - Q_C^0 - p_C^0) \\ &= \int \prod_{i=1}^n [d^4 q_i \delta(q_i^2 - m_i^2) \Theta(q_i^0)] \delta^3\left(\sum_C \vec{q}_i + \vec{p}_C\right) \delta\left(Q_M^0 - \sum_C q_i^0 - p_C^0\right). \end{aligned}$$

This can be recast into a better form by inserting the identity

$$\begin{aligned} 1 &= \int \prod_{i=1}^n \left[d^4 p_i \delta^3\left(\vec{p}_i - u\vec{q}_i + \frac{1}{2n_C + n_N} \vec{K}\right) \delta\left(p_i^0 - \sqrt{\vec{p}_i^2 + m_i^2}\right) \right] \\ &= \int \prod_{i=1}^n \left[d^4 p_i \delta^3(\vec{p}_i - u\vec{q}_i + \vec{\kappa}) \delta\left(p_i^0 - \sqrt{\vec{p}_i^2 + m_i^2}\right) \right] \end{aligned} \quad (79)$$

with the abbreviation

$$\vec{\kappa} = \frac{\vec{K}}{2n_C + n_N},$$

by using the definition of u written as

$$\begin{aligned} 1 &= \int du \delta \left[\sqrt{M^2 + \left(u \sum_C \vec{q}_i - n_C \vec{\kappa}\right)^2} \right. \\ &\quad \left. - \sum_{C,N} \sqrt{m_i^2 + (u\vec{q}_i - \vec{\kappa})^2} - K^0 \right] \left(\frac{\vec{p}_C \vec{p}_C}{p_C^0} - \sum_{C,N} \frac{\vec{p}_i \vec{q}_i}{p_i^0} \right) \end{aligned} \quad (80)$$

and by expressing the δ -function fixing Q_M^0 in terms of the kinematically relevant variables q_i^0 and p_C^0 . This then yields

$$\begin{aligned}
& \int \prod_{i=1}^n \frac{d^3 q_i}{2q_i^0} \delta^3(\vec{Q}_M) \delta(Q_M^0 - Q_C^0 - p_C^0) \\
&= \int du \prod_{i=1}^n \left[d^4 q_i d^4 p_i \delta(q_i^2 - m_i^2) \Theta(q_i^0) \delta^3(\vec{p}_i - u\vec{q}_i + \vec{\kappa}) \delta\left(p_i^0 - \sqrt{\vec{p}_i^2 + m_i^2}\right) \right] \\
&\quad \times \delta\left(\sqrt{M^2 + \left(u \sum_C \vec{q}_i - n_C \vec{\kappa}\right)^2} - \sum_{C,N} \sqrt{m_i^2 + (u\vec{q}_i - \vec{\kappa})^2} - K^0\right) \\
&\quad \times \delta^3\left(\sum_C \vec{q}_i + \vec{p}_C\right) \delta\left(\sqrt{M^2 + \left(\sum_C \vec{q}_i\right)^2} - \sum_{C,N} q_i^0\right) \times \left[\frac{\vec{p}_C \vec{p}_C}{p_C^0} - \sum_{C,N} \frac{\vec{p}_i \vec{q}_i}{p_i^0}\right].
\end{aligned}$$

Integrating over $d^3 q_i$ and dq_i^0 , using $\delta(x^2 - x_0^2) \Theta(x) = \frac{1}{2x_0} \delta(x - x_0)$, and integrating over u yields

$$\begin{aligned}
& \int \prod_{i=1}^n \frac{d^3 q_i}{2q_i^0} \delta^3(\vec{Q}_M) \delta(Q_M^0 - Q_C^0 - p_C^0) \\
&= \int du \prod_{i=1}^n \left[d^4 p_i \delta\left(p_i^0 - \sqrt{\vec{p}_i^2 + m_i^2}\right) \frac{1}{u^3} \frac{1}{2\sqrt{\frac{1}{u^2} (\vec{p}_i + \vec{\kappa})^2 + m_i^2}} \right] \\
&\quad \times \delta^3\left(\frac{1}{u} \left[\sum_C \vec{p}_i + n_C \vec{\kappa} + u\vec{p}_C\right]\right) \\
&\quad \times \delta\left(\sqrt{M^2 + \frac{1}{u^2} \left[\sum_C \vec{p}_i + n_C \vec{\kappa}\right]^2} - \sum_{C,N} \sqrt{m_i^2 + \frac{1}{u^2} [\vec{p}_i + \vec{\kappa}]^2}\right) \\
&\quad \times \delta\left(\sqrt{M^2 + \left[\sum_C \vec{p}_i\right]^2} - \sum_{C,N} \sqrt{m_i^2 + \vec{p}_i^2} - K^0\right) \times \left[\frac{\vec{p}_C \vec{p}_C}{p_C^0} - \sum_{C,N} \frac{\vec{p}_i (\vec{p}_i + \vec{\kappa})}{u p_i^0}\right].
\end{aligned}$$

$$\begin{aligned}
&= \int \prod_{i=1}^n \left[d^4 p_i \delta \left(p_i^0 - \sqrt{\vec{p}_i^2 + m_i^2} \right) \frac{1}{u^3} \frac{1}{2\sqrt{\frac{1}{u^2} (\vec{p}_i + \vec{\kappa})^2 + m_i^2}} \right] \\
&\quad \times u^3 \delta^3 \left(\sum_C \vec{p}_i + \vec{p}_C \right) \delta \left(\sqrt{M^2 + \left[\sum_C \vec{p}_i \right]^2} - \sum_{C,N} \sqrt{m_i^2 + \vec{p}_i^2} - K^0 \right) \\
&\quad \times \left[\frac{\vec{p}_C \vec{p}_C}{p_C^0} - \sum_{C,N} \frac{\vec{p}_i (\vec{p}_i + \vec{\kappa})}{u p_i^0} \right] \left[\frac{u}{\frac{\vec{p}_C^2}{p_C^0} - \sum_{C,N} \frac{\vec{q}_i^2}{q_i^0}} \right],
\end{aligned}$$

where in the integration over u the second last δ -function of the line above has been used. Furthermore, in this transformation, an identity similar to (80), arising when defining u in terms of p_i , has been employed. A rearrangement of terms and a suitable transformation of the last δ -function in terms of P_M yields

$$\begin{aligned}
&\int \prod_{i=1}^n \frac{d^3 q_i}{2q_i^0} \delta^3(Q_M) \delta(Q_M^0 - Q_C^0 - p_C^0) \\
&= \int \prod_{i=1}^n \left[d^4 p_i \delta(p_i^2 - m_i^2) \Theta(p_i^0) \frac{1}{u^3} \frac{\sqrt{\vec{p}_i^2 + m_i^2}}{\sqrt{\frac{1}{u^2} (\vec{p}_i + \vec{\kappa})^2 + m_i^2}} \right] \\
&\quad \times u^4 \delta^3 \left(\sum_C \vec{p}_i + \vec{p}_C \right) \delta(p_C^0 - P_C^0 - P_N^0 - K^0) \frac{\frac{\vec{p}_C \vec{p}_C}{p_C^0} - \sum_{C,N} \frac{\vec{p}_i \vec{q}_i}{p_i^0}}{\frac{\vec{p}_C^2}{p_C^0} - \sum_{C,N} \frac{\vec{q}_i^2}{q_i^0}} \\
&= \int \prod_{i=1}^n [d^4 p_i \delta(p_i^2 - m_i^2) \Theta(p_i^0)] \delta^3(\vec{P}_M) \delta(P_M^0 - P_C^0 - p_C^0) \\
&\quad \times \frac{1}{u^{3n-4}} \frac{\frac{\vec{p}_C \vec{p}_C}{p_C^0} - \sum_{C,N} \frac{\vec{p}_i \vec{q}_i}{p_i^0}}{\frac{\vec{p}_C^2}{p_C^0} - \sum_{C,N} \frac{\vec{q}_i^2}{q_i^0}} \prod_{i=1}^n \left[\frac{p_i^0}{q_i^0} \right].
\end{aligned}$$

Here, the identity

$$q_i^0 = \sqrt{\frac{1}{u^2} (\vec{p}_i + \vec{\kappa})^2 + m_i^2}$$

has been used. Reversing the procedure allows to express the phase space element through the undressed final state momenta as

$$\begin{aligned}
d\Phi &= (2\pi)^4 d\Phi_q d\Phi_k \delta^3(\vec{Q}_M) \delta(Q_M^0 - Q_C^0 - p_C^0) \frac{m_M^3}{M^2 (P_C^0 + P_N^0 + K^0)} \\
&\quad \times u^{3n-4} \frac{\frac{\vec{p}_C^2}{p_C^0} - \sum_{C,N} \frac{\vec{q}_i^2}{q_i^0}}{\frac{\vec{p}_C \vec{p}_C}{p_C^0} - \sum_{C,N} \frac{\vec{p}_i \vec{q}_i}{p_i^0}} \prod_{i=1}^n \left[\frac{q_i^0}{p_i^0} \right].
\end{aligned}$$

B.2.2 Final state multipoles

The transformation will be done using the same techniques as above. Starting from

$$\begin{aligned} & \int \prod_{i=1}^n \frac{d^3 q_i}{2q_i^0} \delta^3(\vec{Q}_M) \delta(Q_M^0 - Q_C^0) \\ &= \int \prod_{i=1}^n [d^4 q_i \delta(q_i^2 - m_i^2) \Theta(q_i^0)] \delta^3\left(\sum_C \vec{q}_i\right) \delta\left(Q_M^0 - \sum_C q_i^0\right). \end{aligned}$$

Again, similar identities to (79) and (80) will be used, but due to the different mapping scheme they now read

$$1 = \int \prod_{i=1}^n \left[d^4 p_i \delta^3(\vec{p}_i - u\vec{q}_i) \delta\left(p_i^0 - \sqrt{\vec{p}_i^2 + m_i^2}\right) \right] \quad (81)$$

and

$$1 = \int du \delta \left[\sqrt{M^2 + \left(u \sum_N \vec{q}_i + \vec{K}\right)^2} - \sum_{C,N} \sqrt{m_i^2 + u^2 \vec{q}_i^2} - K^0 \right] \left(\frac{\vec{p}_N \vec{p}_N}{p_N^0} - \sum_{C,N} \frac{\vec{p}_i \vec{q}_i}{p_i^0} \right). \quad (82)$$

And, as before, the δ -function over Q_M^0 is expressed in the kinematically relevant variables q_i^0 . This then yields

$$\begin{aligned} & \int \prod_{i=1}^n \frac{d^3 q_i}{2q_i^0} \delta^3(\vec{Q}_M) \delta(Q_M^0 - Q_C^0) \\ &= \int du \prod_{i=1}^n \left[d^4 q_i d^4 p_i \delta(q_i^2 - m_i^2) \Theta(q_i^0) \delta^3(\vec{p}_i - u\vec{q}_i) \delta\left(p_i^0 - \sqrt{\vec{p}_i^2 + m_i^2}\right) \right] \\ & \quad \times \delta \left(\sqrt{M^2 + \left(u \sum_N \vec{q}_i + \vec{K}\right)^2} - \sum_{C,N} \sqrt{m_i^2 + u^2 \vec{q}_i^2} - K^0 \right) \\ & \quad \times \delta^3\left(\sum_C \vec{q}_i\right) \delta\left(\sqrt{M^2 + \left(\sum_N \vec{q}_i\right)^2} - \sum_{C,N} q_i^0\right) \times \left[\frac{\vec{p}_N \vec{p}_N}{p_N^0} - \sum_{C,N} \frac{\vec{p}_i \vec{q}_i}{p_i^0} \right]. \end{aligned}$$

Integrating over d^4q_i and u yields

$$\begin{aligned}
& \int \prod_{i=1}^n \frac{d^3q_i}{2q_i^0} \delta^3(\vec{Q}_M) \delta(Q_M^0 - Q_C^0) \\
&= \int du \prod_{i=1}^n \left[d^4p_i \delta\left(p_i^0 - \sqrt{\vec{p}_i^2 + m_i^2}\right) \frac{1}{u^3} \frac{1}{2\sqrt{\frac{1}{u^2}\vec{p}_i^2 + m_i^2}} \right] \delta^3\left(\frac{1}{u} \sum_C \vec{p}_i\right) \\
&\quad \times \delta\left(\sqrt{M^2 + \frac{1}{u^2} \left[\sum_N \vec{p}_i\right]^2} - \sum_{C,N} \sqrt{\frac{1}{u^2}\vec{p}_i^2 + m_i^2}\right) \\
&\quad \times \delta\left(\sqrt{M^2 + \left[\sum_N \vec{p}_i + \vec{K}\right]^2} - \sum_{C,N} \sqrt{m_i^2 + \vec{p}_i^2} - K^0\right) \times \left[\frac{\vec{p} \cdot \vec{p}}{p^0} - \sum_{C,N} \frac{\vec{p}_i^2}{up_i^0}\right] \\
&= \int \prod_{i=1}^n \left[d^4p_i \delta(p_i^2 - m_i^2) \Theta(p_i^0) \frac{1}{u^3} \frac{\sqrt{\vec{p}_i^2 + m_i^2}}{\sqrt{\frac{1}{u^2}\vec{p}_i^2 + m_i^2}} \right] u^3 \delta^3\left(\sum_C \vec{p}_i\right) \\
&\quad \times \delta\left(\sqrt{M^2 + \left[\sum_N \vec{p}_i + \vec{K}\right]^2} - \sum_{C,N} \sqrt{m_i^2 + \vec{p}_i^2} - K^0\right) \\
&\quad \times \left[\frac{\vec{p} \cdot \vec{p}}{p^0} - \sum_{C,N} \frac{\vec{p}_i^2}{up_i^0}\right] \left[\frac{u}{\vec{p}^2 - \sum_{C,N} \frac{\vec{q}_i^2}{q_i^0}}\right]
\end{aligned}$$

where, again, the second last δ -function has been used in the integration over u . Additionally, an identity similar to (82), arising when defining u in terms of p_i , has been used. Rearranging terms leads to

$$\begin{aligned}
& \int \prod_{i=1}^n \frac{d^3q_i}{2q_i^0} \delta^3(\vec{Q}_M) \delta(Q_M^0 - Q_C^0) \\
&= \int \prod_{i=1}^n \left[d^4p_i \delta(p_i^2 - m_i^2) \Theta(p_i^0) \frac{1}{u^3} \frac{\sqrt{\vec{p}_i^2 + m_i^2}}{\sqrt{\frac{1}{u^2}\vec{p}_i^2 + m_i^2}} \right] \\
&\quad \times u^4 \delta^3(\vec{P}_C) \delta(p_N^0 - P_C^0 - P_N^0 - K^0) \frac{\frac{\vec{p}_N \cdot \vec{p}_N}{p_N^0} - \sum_{C,N} \frac{\vec{p}_i \cdot \vec{q}_i}{p_i^0}}{\frac{\vec{p}_N^2}{p_N^0} - \sum_{C,N} \frac{\vec{q}_i^2}{q_i^0}} \\
&= \int \prod_{i=1}^n \left[d^4p_i \delta(p_i^2 - m_i^2) \Theta(p_i^0) \right] \delta^3(\vec{P}_M) \delta(P_M^0 - P_C^0) \frac{1}{u^{3n-4}} \frac{\frac{\vec{p}_N \cdot \vec{p}_N}{p_N^0} - \sum_{C,N} \frac{\vec{p}_i \cdot \vec{q}_i}{p_i^0}}{\frac{\vec{p}_N^2}{p_N^0} - \sum_{C,N} \frac{\vec{q}_i^2}{q_i^0}} \prod_{i=1}^n \left[\frac{p_i^0}{q_i^0} \right]
\end{aligned}$$

where the identity

$$q_i^0 = \sqrt{\frac{1}{u^2} \vec{p}_i^2 + m_i^2}$$

has been used. Reversing the procedure allows to express the phase space element through the undressed final state momenta as

$$\begin{aligned} d\Phi &= d\Phi_q d\Phi_k (2\pi)^4 \delta^3(\vec{Q}_M) \delta(Q_M^0 - Q_C^0) \frac{m_M^3}{M^2(P^0 + P_N^0 + K^0)} \\ &\times u^{3n-4} \frac{\frac{\vec{p}_N^2}{p_N^0} - \sum_{C,N} \frac{\vec{q}_i^2}{q_i^0}}{\frac{\vec{p}_N \vec{p}_N}{p_N^0} - \sum_{C,N} \frac{\vec{p}_i \vec{q}_i}{p_i^0}} \prod_{i=1}^n \left[\frac{q_i^0}{p_i^0} \right]. \end{aligned}$$

C Details on the photon generation

In this section the generation of the photon distribution is detailed.

C.1 Average photon multiplicity

The average photon multiplicity \bar{n} is the average of the Poisson distribution before it is corrected by the various weights. It is therefore not immediately connected to the true average photon multiplicity of the final event. Nonetheless, it is an integral part of the generation procedure. An analytical result in closed form is available for both dipoles and multipoles. However, the calculations for multipoles are more involved as the integrations do not nicely separate as they do in the dipole case in the chosen frame. Thus, as a starting point the analytical result for the dipole in its rest frame will be given. It reads

$$\bar{n} = \int_{\omega_{\min}}^{\omega_{\max}} \frac{d^3k}{k^0} \tilde{S}_q(k) = -\frac{\alpha}{\pi} Z_1 Z_2 \theta_1 \theta_2 \ln \frac{\omega_{\max}}{\omega_{\min}} \left(\frac{1 + \beta_1 \beta_2}{\beta_1 + \beta_2} \ln \frac{(1 + \beta_1)(1 + \beta_2)}{(1 - \beta_1)(1 - \beta_2)} - 2 \right),$$

where ω_{\min} is the infrared cut-off and ω_{\max} is the maximal kinematically allowed photon energy. The latter can be determined by setting the rescaling parameter u to zero in Eqs. (36) and (41), respectively, and by assuming single photon emission. Additionally, $\beta_i = \frac{|\vec{p}_i|}{E_i}$.

In the case of a multipole, the integral over the photon energy can still be separated, as long as the soft photon region is sufficiently well-behaved. This is the case, if $\Theta(k, \Omega)$ forms an isotropic hypersurface in the frame of the integration. However, the angular integration still remains to be done:

$$\begin{aligned} \bar{n} &= \int \frac{d^3k}{k^0} \Theta(k, \Omega) \tilde{S}_q(k) \\ &= \frac{\alpha}{4\pi^2} \sum_{i < j} Z_i Z_j \theta_i \theta_j \int \frac{d^3k}{k^0} \Theta(k, \Omega) \left(\frac{q_i}{(q_i \cdot k)} - \frac{q_j}{(q_j \cdot k)} \right)^2 \\ &= \frac{\alpha}{4\pi^2} \ln \frac{\omega_{\max}}{\omega_{\min}} \sum_{i < j} Z_i Z_j \theta_i \theta_j \left(8\pi - \int d\Omega \frac{2(q_i \cdot q_j)}{(q_i \cdot e_k)(q_j \cdot e_k)} \right). \end{aligned}$$

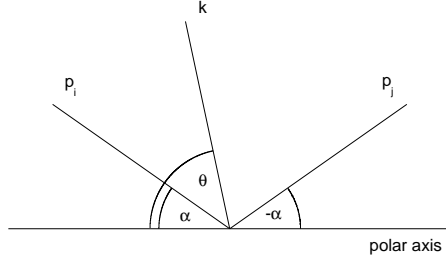


Figure 12: *Sketch of how the axes are chosen in the angular integration in multipoles.*

Choosing different orientations of the polar axes for each interference term of every constituent dipole, all angular integrations can be done analytically. Although this may sound like quite an *ad-hoc* procedure, it is completely valid and simplifies the integration immensely. The orientation for each of the interference terms is thus chosen to be such that both momenta lie symmetrically in the unit sphere, both forming an angle α_{ij} with the polar axis, see Fig. 12. Therefore, by this choice,

$$\begin{aligned} (q_i \cdot q_j) &= E_i E_j (1 - a_i a_j + b_i b_j) \\ (q_i \cdot e_k) &= E_i (1 - a_i \sin \varphi \sin \theta - b_i \cos \theta) \\ (q_j \cdot e_k) &= E_j (1 - a_j \sin \varphi \sin \theta + b_j \cos \theta) , \end{aligned}$$

where e_k^μ again is $\frac{1}{k^0} k^\mu$ with $e_k^2 = 0$, cf. Eq. (51), and the further parameters are given by

$$a_{i,j} = \beta_{i,j} \sin \alpha_{ij} \quad \text{and} \quad b_{i,j} = \beta_{i,j} \cos \alpha_{ij} .$$

With these choices the last integral reads

$$\begin{aligned} &\int d\Omega \frac{E_i E_j}{(q_i \cdot e_k)(q_j \cdot e_k)} \\ &= \int_0^{2\pi} d\varphi \int_0^\pi d\theta \sin \theta \frac{1}{(1 - a_i \sin \varphi \sin \theta - b_i \cos \theta)(1 - a_j \sin \varphi \sin \theta + b_j \cos \theta)} . \end{aligned}$$

Using the decomposition

$$\begin{aligned} &\frac{1}{b_j (1 - a_i \sin \varphi \sin \theta - b_i \cos \theta)} - \frac{1}{b_i (1 - a_j \sin \varphi \sin \theta + b_j \cos \theta)} \\ &= \frac{(b_i - b_j) + 2b_i b_j \cos \theta}{b_i b_j (1 - a_i \sin \varphi \sin \theta - b_i \cos \theta)(1 - a_j \sin \varphi \sin \theta + b_j \cos \theta)} \end{aligned}$$

and $a_i b_j = a_j b_i$, this can be easily integrated giving

$$\begin{aligned} & \int d\Omega \frac{E_i E_j}{(q_i \cdot e_k)(q_j \cdot e_k)} \\ &= 2\pi \left[\frac{b_i}{\sqrt{B^2 C_i - ABD_i + A^2 E_i}} \ln \frac{A+B}{A-B} \frac{\sqrt{C_i - D_i + E_i} + \frac{B(2C_i - D_i) - A(D_i - 2E_i)}{2\sqrt{B^2 C_i - ABD_i + A^2 E_i}}}{\sqrt{C_i + D_i + E_i} + \frac{B(2C_i + D_i) - A(D_i + 2E_i)}{2\sqrt{B^2 C_i - ABD_i + A^2 E_i}}} \right. \\ & \quad \left. - \frac{b_j}{\sqrt{B^2 C_j - ABD_j + A^2 E_j}} \ln \frac{A+B}{A-B} \frac{\sqrt{C_j - D_j + E_j} + \frac{B(2C_j - D_j) - A(D_j - 2E_j)}{2\sqrt{B^2 C_j - ABD_j + A^2 E_j}}}{\sqrt{C_j + D_j + E_j} + \frac{B(2C_j + D_j) - A(D_j + 2E_j)}{2\sqrt{B^2 C_j - ABD_j + A^2 E_j}}} \right], \end{aligned}$$

with

$$\begin{aligned} A &= b_i - b_j \\ B &= 2b_i b_j \\ C_{i,j} &= 1 - a_{i,j} \\ D_{i,j} &= \mp b_{i,j} \\ E_{i,j} &= a_{i,j}^2 + b_{i,j}^2. \end{aligned}$$

Upon closer examination it can be seen that for $\alpha_{ij} \rightarrow 0$ the result of the dipole case is recovered.

C.2 Photon energy

Due to the decomposition of the integration over the photon energy and the integration over the unit sphere, the photon energy distribution and the photon angular distribution can be generated separately. Of course, this independence of distributions is no longer true after the reweighting procedure, but it alleviates the generation of the crude distribution.

In the implementation presented here, the photon energy is distributed according to $\frac{1}{k^0}$, generated through

$$k^0 = \omega_{\min} \left(\frac{\omega_{\max}}{\omega_{\min}} \right)^{\mathcal{R}}$$

where \mathcal{R} is a uniformly distributed random number on the interval $[0, 1]$.

C.3 Photon angles

Similar to all other parts of the photon distribution, the photon angles are also generated according to $\tilde{S}_q(k)$. For this, the relevant function is recast into the form

$$\begin{aligned} & - \left(\frac{q_i}{(q_i \cdot e_k)} - \frac{q_j}{(q_j \cdot e_k)} \right)^2 \\ &= - \frac{1 - \beta_i^2}{(1 - \beta_i \cos \theta)^2} + \frac{2(1 + \beta_i \beta_j)}{(1 - \beta_i \cos \theta)(1 + \beta_j \cos \theta)} - \frac{1 - \beta_j^2}{(1 + \beta_j \cos \theta)^2}, \end{aligned}$$

where θ is some polar angle w.r.t. the dipole axis in the dipole rest frame. In this frame, the generation of the azimuthal is trivial - it just follows a flat distribution in $[0, 2\pi]$. The polar distribution above can be bound from above through the interference term. This allows to generate the true distribution by generating the angle according to the interference term and applying a hit-or-miss rejection. The interference term can be decomposed analogously to the general case above into two independent terms according to

$$\frac{1}{(1 - \beta_i \cos \theta)(1 + \beta_j \cos \theta)} = \frac{\beta_i \beta_j}{\beta_i + \beta_j} \left(\frac{1}{\beta_j(1 - \beta_i \cos \theta)} - \frac{1}{\beta_i(1 + \beta_j \cos \theta)} \right).$$

The cosine of the polar angle, $\cos \theta$, is then generated to either of the two terms, i.e. it is generated according to $(1 - \beta_i \cos \theta)^{-1}$ with probability

$$P_i = \frac{\ln \frac{1+\beta_i}{1-\beta_i}}{\ln \frac{1+\beta_i}{1-\beta_i} + \ln \frac{1+\beta_j}{1-\beta_j}}$$

and according to $(1 + \beta_j \cos \theta)^{-1}$ with probability $P_j = 1 - P_i$, selected through a random number. These angles can be generated by

$$\cos \theta = \frac{1}{\beta_i} \left[1 - (1 + \beta_i) \left(\frac{1 - \beta_i}{1 + \beta_i} \right)^{\mathcal{R}} \right]$$

in the former case and

$$\cos \theta = -\frac{1}{\beta_j} \left[1 - (1 - \beta_j) \left(\frac{1 + \beta_j}{1 - \beta_j} \right)^{\mathcal{R}} \right]$$

in the latter. \mathcal{R} again is a uniformly distributed random number on $[0, 1]$. The correction weight for obtaining the full distribution reads

$$W = \frac{-\frac{1-\beta_i^2}{(1-\beta_i \cos \theta)^2} + \frac{2(1+\beta_i \beta_j)}{(1-\beta_i \cos \theta)(1+\beta_j \cos \theta)} - \frac{1-\beta_j^2}{(1+\beta_j \cos \theta)^2}}{\frac{2(1+\beta_i \beta_j)}{(1-\beta_i \cos \theta)(1+\beta_j \cos \theta)}} \leq 1.$$

The azimuthal angle φ is distributed uniformly.

C.4 Photons from multipoles

In a multipole configuration again the photons are generated according to $\tilde{S}_q(k)$. The integral over photon energies can still be separated from the angular integrations, decoupling the generation of the energy of a single photon as above. However, its angular distribution is very complex. But due to

$$\tilde{S}_q(k) = \sum_{i < j} \tilde{S}(q_i, q_j, k)$$

the photon angles are distributed according to

$$- \sum_{i < j} |Z_i Z_j \theta_i \theta_j| \left(\frac{q_i}{(q_i \cdot e_k)} - \frac{q_j}{(q_j \cdot e_k)} \right)^2.$$

This is nothing but a sum of angular distributions of different dipoles which are not in their respective rest frame.

Subsequently, one of those constituent dipoles is chosen with the probability

$$P_{ij} = \frac{|\bar{n}_{ij}|}{\sum_{i < j} |\bar{n}_{ij}|} = \frac{\left| \int \frac{d^3 k}{k^0} \tilde{S}(q_i, q_j, k) \right|}{\sum_{i < j} \left| \int \frac{d^3 k}{k^0} \tilde{S}(q_i, q_j, k) \right|}.$$

Then, photon angle generation can proceed as above in the rest frame of the dipole. To obtain the right distribution in the rest frame of the overall multipole, a null-vector of unit length is created in the rest frame of the dipole using the newly generated angles φ and θ . Then this null vector is boosted into the rest frame of the multipole. It now has the angular distribution according to its constituent dipole in this frame. Since it is a null vector it has the properties of a photon and only needs to be rescaled to the energy generated earlier.

D Massive dipole splitting functions

The massive dipole splitting functions are needed for the calculation of the approximation to the infrared subtracted single hard photon emission matrix element $\tilde{\beta}_1^1$. They are taken directly from [17] for spin- $\frac{1}{2}$ emitters and are generalised from [19] for all other cases. Problems arising during this generalisation are related to the fact that these splitting functions for spin-1 particles are only given for massless gluons and that all initial states are considered massless as well. The extension to radiation off massive spin-1 particles is rather straight forward by augmentation with a simple mass term. The extension to massive initial states is less clear since decay matrix elements are far off the massless initial state limit. However, the decaying particle is always much more massive than its decay products when those are supposed to emit hard bremsstrahlung. Thus, photons are predominantly emitted at large angles to the initial state resulting in negligible contributions from these splitting functions. Hence, they can safely be omitted.

Also, velocity factors from [19] have been omitted. They were introduced to facilitate the analytic integration and change neither the infrared nor the quasi-collinear limit. They only result in a different interpolation inbetween. The same is true for the factor R_{ij} in the massive fermion splitting function of [17]. Nonetheless, here this factor is kept because of the direct applicability of these splitting functions to the completely massive splitting.

Three cases need to be differentiated regarding the state, initial or final, the emitter and spectator are in. The fourth case where both emitter and spectator are in the initial state lies outside the present applicability of this program, it will therefore be omitted.

To repeat the notation, p_i is the 4-momentum of the emitter, p_j that of the spectator and k is the emitted photon. All massive dipole splitting functions will be given, in that order, for spin-0, spin- $\frac{1}{2}$ and spin-1 emitters. Since there are no massive dipole splitting functions available for emitters of spin- $\frac{3}{2}$ or spin-2, their emissions have to be described by the soft limit only. Of course, it is always possible to implement exact process specific matrix elements.

Final State Emitter, Final State Spectator

$$\begin{aligned}
g_{ij}(p_i, p_j, k) &= g_{ij}^{(\text{soft})}(p_i, p_j, k) \\
&= \frac{1}{(p_i \cdot k) R_{ij}(y_{ij})} \left[\frac{2}{1 - z_{ij}(1 - y_{ij})} - 1 - z_{ij} - \frac{m_i^2}{(p_i \cdot k)} \right] \\
&= \frac{1}{(p_i \cdot k)} \left[\frac{2}{1 - z_{ij}(1 - y_{ij})} + \frac{2}{1 - z_{kj}(1 - y_{ij})} + 2z_{ij}z_{kj} - 4 - \frac{m_i^2}{(p_i \cdot k)} \right]
\end{aligned}$$

with

$$\begin{aligned}
y_{ij} &= \frac{p_i k}{p_i p_j + p_i k + p_j k} \\
z_{ij} &= \frac{p_i p_j}{p_i p_j + p_j k} \\
z_{kj} &= 1 - z_{ij} \\
v_{ik,j} &= \frac{1}{2} R_{ij}(y_{ij}) \frac{\sqrt{\lambda(P_{ij}^2, m_i^2, m_j^2)}}{(p_i + k) \cdot p_j}
\end{aligned}$$

and

$$R_{ij}(x) = \frac{\sqrt{(2m_j^2 + \bar{P}_{ij}^2(1-x))^2 - 4P_{ij}^2 m_j^2}}{\sqrt{\lambda(P_{ij}^2, m_i^2, m_j^2)}}$$

with

$$\begin{aligned}
P_{ij} &= p_i + p_j + k \\
\bar{P}_{ij}^2 &= P_{ij}^2 - m_i^2 - m_j^2 = 2(p_i p_j + p_i k + p_j k)
\end{aligned}$$

wherein the photon is massless, $\lambda(x, y, z)$ is the Kallen-function.

Final State Emitter, Initial State Spectator

$$\begin{aligned}
g_{ij}(p_i, p_j, k) &= g_{ij}^{(\text{soft})}(p_i, p_j, k) \\
&= \frac{1}{(p_i \cdot k) x_{ij}} \left[\frac{2}{2 - x_{ij} - z_{ij}} - 1 - z_{ij} - \frac{m_i^2}{(p_i \cdot k)} \right] \\
&= \frac{1}{(p_i \cdot k) x_{ij}} \left[\frac{2}{2 - x_{ij} - z_{ij}} + \frac{2}{2 - x_{ij} - z_{kj}} + 2z_{ij}z_{kj} - 4 - \frac{m_i^2}{(p_i \cdot k)} \right]
\end{aligned}$$

$s_1 s_2$	$X(p_1, s_1; p; p_2, s_2; c_L, c_R)$
++	$\mu_1 \mu_2 \eta^2 c_L + \mu^2 \eta_1 \eta_2 c_R + c_R S(+; p_1, p) S(-; p, p_2)$
+-	$c_L \mu_1 \eta S(+; p, p_2) + c_R \mu_2 \eta S(+; p_1, p)$

Table 3: X -Functions for different helicity combinations. Missing combinations can be obtained using the simultaneous replacements $+\leftrightarrow-$ and $L\leftrightarrow R$.

with

$$\begin{aligned}
x_{ij} &= \frac{p_i p_j + p_j k - p_i k}{p_i p_j + p_j k} \\
z_{ij} &= \frac{p_i p_j}{p_i p_j + p_j k} \\
z_{kj} &= 1 - z_{ij}
\end{aligned}$$

Initial State Emitter, Final State Spectator

The emitting particle is always assumed to be much heavier than its decay products resulting in its contributions to the real emission corrections to be negligible. Thus,

$$g_{ij}(p_i, p_j, k) = g_{ij}^{(\text{soft})}(p_i, p_j, k)$$

is set irrespective of the emitter's spin.

E Basic building blocks For matrix element calculations

In this Appendix a short summary on the definitions of the basic building blocks (cf. [20,21]) for the calculations of exact matrix elements will be given. Additionally, techniques to incorporate propagators into that scheme will be reviewed.

X -Function

The X -function is a contraction over a fermionic current coupled to a vector with an arbitrary structure of the vertex.

$$X(p_1, s_1; p; p_2, s_2; c_L, c_R) = \bar{u}(p_1, s_1) \not{p} [c_L P_L + c_R P_R] u(p_2, s_2),$$

where $u(p_i, s_i)$ may be a particle or anti-particle spinor, $P_L = \frac{1-\gamma^5}{2}$ and $P_R = \frac{1+\gamma^5}{2}$. The vector p^μ dotted into the γ -matrix may be a momentum vector or a polarisation vector. For the explicit calculation of the X -Function see Table 3.

$s_1 s_2$	$Y(p_1, s_1; p_2, s_2; c_L, c_R)$
++	$c_R \mu_1 \eta_2 + c_L \mu_2 \eta_1$
+-	$c_L S(+; p_1, p_2)$

Table 4: Y -Functions for different helicity combinations. Missing combinations can be obtained using the simultaneous replacements $+\leftrightarrow-$ and $L\leftrightarrow R$.

$s_1 s_2 s_3 s_4$	$Z(p_1, s_1; p_2, s_2; p_3, s_3; p_4, s_4; c_L^{12}, c_R^{12}; c_L^{34}, c_R^{34})$
++++	$2 [S(+; p_3, p_1)S(-; p_2, p_4)c_R^{12}c_R^{34} + \mu_1\mu_2\eta_3\eta_4c_L^{12}c_R^{34} + \mu_3\mu_4\eta_1\eta_2c_R^{12}c_L^{34}]$
+++-	$2\eta_2c_R^{12} [S(+; p_1, p_4)\mu_3c_L^{34} + S(+; p_1, p_3)\mu_4c_R^{34}]$
++-+	$2\eta_1c_R^{12} [S(-; p_3, p_2)\mu_4c_L^{34} + S(-; p_4, p_2)\mu_3c_R^{34}]$
++--	$2 [S(+; p_4, p_1)S(-; p_2, p_3)c_R^{12}c_L^{34} + \mu_1\mu_2\eta_3\eta_4c_L^{12}c_R^{34} + \mu_3\mu_4\eta_1\eta_2c_R^{12}c_L^{34}]$
+ - ++	$2\eta_4c_R^{34} [S(+; p_1, p_3)\mu_2c_R^{12} + S(+; p_2, p_3)\mu_1c_L^{12}]$
+ - +-	0
+ - -+	$-2 [\mu_1\mu_4\eta_2\eta_3c_L^{12}c_L^{34} + \mu_2\mu_3\eta_1\eta_4c_R^{12}c_R^{34} - \mu_1\mu_3\eta_2\eta_4c_L^{12}c_R^{34} - \mu_2\mu_4\eta_1\eta_3c_R^{12}c_L^{34}]$
+ - --	$2\eta_3c_R^{34} [S(+; p_4, p_2)\mu_1c_L^{12} + S(+; p_1, p_4)\mu_2c_R^{12}]$

Table 5: Z -Functions for different helicity combinations. Missing combinations can be obtained using the simultaneous replacements $+\leftrightarrow-$ and $L\leftrightarrow R$.

Y-Function

The Y -function is the pendant of the X -function when the fermionic current is coupling to a scalar rather than a vector.

$$Y(p_1, s_1; p_2, s_2; c_L, c_R) = \bar{u}(p_1, s_1) [c_L P_L + c_R P_R] u(p_2, s_2).$$

Its explicit calculation is shown in Table 4.

Z-Function

The Z -function is a contraction over two fermionic currents connected by a massless gauge boson (cf. Table 5).

$$\begin{aligned} Z(p_1, s_1; p_2, s_2; p_3, s_3; p_4, s_4; c_L^{12}, c_R^{12}; c_L^{34}, c_R^{34}) \\ = \bar{u}(p_1, s_1)\gamma^\mu [c_L^{12} P_L + c_R^{12} P_R] u(p_2, s_2)\bar{u}(p_3, s_3)\gamma_\mu [c_L^{34} P_L + c_R^{34} P_R] u(p_4, s_4). \end{aligned}$$

S-Function

For the calculation of the above spinorial products it is useful to define the S -Function

$$S(s; p_1, p_2) = \bar{u}(p_1, s)u(p_2, -s).$$

Its two possible forms for given p_1 and p_2 are

$$S(+; p_1, p_2) = 2 \frac{(p_1 \cdot k_0)(p_2 \cdot k_1) - (p_1 \cdot k_1)(p_2 \cdot k_0) - i\epsilon_{\alpha\beta\gamma\delta} p_1^\alpha p_2^\beta k_0^\gamma k_1^\delta}{\eta_1 \eta_2}$$

$$S(-; p_1, p_2) = -2 \frac{(p_1 \cdot k_0)(p_2 \cdot k_1) - (p_1 \cdot k_1)(p_2 \cdot k_0) + i\epsilon_{\alpha\beta\gamma\delta} p_1^\alpha p_2^\beta k_0^\gamma k_1^\delta}{\eta_1 \eta_2},$$

where k_0 is an arbitrary null vector ($k_0^2 = 0$) and k_1 satisfies the relations $k_1^2 = -1$ and $(k_0 \cdot k_1) = 0$. Furthermore,

$$\eta_i = \sqrt{2(p_i \cdot k_0)}.$$

It is also useful to define the quantity

$$\mu_i = \pm \frac{m_i}{\eta_i},$$

where \pm refers to particles/anti-particles.

Fermionic Propagators

These propagators can be incorporated using the following identity:

$$(\not{p} \pm m) = \frac{1}{2} \sum_s \left[\left(1 \pm \frac{m}{\sqrt{p^2}} \right) u(p, s) \bar{u}(p, s) + \left(1 \mp \frac{m}{\sqrt{p^2}} \right) v(p, s) \bar{v}(p, s) \right].$$

This allows to cut the line and replace it with a sum of external particles

Bosonic Propagators

Bosonic propagators can be incorporated by writing out their Lorentz-structure explicitly. This is trivial in Feynman gauge, if the vector is massless. Massive propagators are best included in unitary gauge, since then no additional goldstone boson exchange has to be included.

References

- [1] T. Sjostrand, S. Mrenna and P. Skands, *A Brief Introduction to PYTHIA 8.1*, Comput. Phys. Commun. **178** (2008), 852–867, [[arXiv:0710.3820 \[hep-ph\]](#)].
- [2] M. Bahr et al., *Herwig++ Physics and Manual*, [arXiv:0803.0883 \[hep-ph\]](#).
- [3] T. Gleisberg et al., *SHERPA 1.alpha, a proof-of-concept version*, JHEP **02** (2004), 056, [[hep-ph/0311263](#)].
- [4] E. Barberio, B. van Eijk and Z. Was, *PHOTOS: A Universal Monte Carlo for QED radiative corrections in decays*, Comput. Phys. Commun. **66** (1991), 115–128.

- [5] G. Nanava and Z. Was, *Scalar QED, NLO and PHOTOS Monte Carlo*, Eur. Phys. J. **C51** (2007), 569–583, [hep-ph/0607019].
- [6] K. Hamilton and P. Richardson, *Simulation of QED radiation in particle decays using the YFS formalism*, JHEP **07** (2006), 010, [hep-ph/0603034].
- [7] Z. Was, P. Golonka and G. Nanava, *PHOTOS Monte Carlo and its theoretical accuracy*, arXiv:0807.2762 [hep-ph].
- [8] D. R. Yennie, S. C. Frautschi and H. Suura, *The infrared divergence phenomena and high-energy processes*, Ann. Phys. **13** (1961), 379–452.
- [9] S. Jadach, B. F. L. Ward and Z. Was, *The precision Monte Carlo event generator KK for two-fermion final states in e^+e^- collisions*, Comput. Phys. Commun. **130** (2000), 260–325, [hep-ph/9912214].
- [10] S. Jadach, B. F. L. Ward and Z. Was, *Coherent exclusive exponentiation for precision Monte Carlo calculations*, Nucl. Phys. Proc. Suppl. **89** (2000), 106–111, [hep-ph/0012124].
- [11] S. Jadach, W. Placzek, M. Skrzypek, B. F. L. Ward and Z. Was, *Precision predictions for (un)stable W^+W^- pair production at and beyond LEP2 energies*, Phys. Rev. **D65** (2002), 093010, [hep-ph/0007012].
- [12] S. Jadach, W. Placzek, M. Skrzypek, B. F. L. Ward and Z. Was, *The Monte Carlo program KoralW version 1.51 and the concurrent Monte Carlo KoralW@YFSWW3 with all background graphs and first order corrections to W pair production*, Comput. Phys. Commun. **140** (2001), 475–512, [hep-ph/0104049].
- [13] C. M. Carloni Calame, S. Jadach, G. Montagna, O. Nicrosini and W. Placzek, *Comparisons of the Monte Carlo programs HORACE and WINHAC for single W -boson production at hadron colliders*, Acta Phys. Polon. **B35** (2004), 1643–1674, [hep-ph/0402235].
- [14] T. Kinoshita, *Mass singularities of Feynman amplitudes*, J. Math. Phys. **3** (1962), 650–677.
- [15] T. D. Lee and M. Nauenberg, *Degenerate Systems and Mass Singularities*, Phys. Rev. **133** (1964), B1549–B1562.
- [16] G. Altarelli and G. Parisi, *Asymptotic Freedom in Parton Language*, Nucl. Phys. **B126** (1977), 298.
- [17] S. Dittmaier, *A general approach to photon radiation off fermions*, Nucl. Phys. **B565** (2000), 69–122, [hep-ph/9904440].
- [18] S. Catani, S. Dittmaier and Z. Trocsanyi, *One-loop singular behaviour of QCD and SUSY QCD amplitudes with massive partons*, Phys. Lett. **B500** (2001), 149–160, [hep-ph/0011222].

- [19] S. Catani, S. Dittmaier, M. H. Seymour and Z. Trocsanyi, *The dipole formalism for next-to-leading order QCD calculations with massive partons*, Nucl. Phys. **B627** (2002), 189–265, [[hep-ph/0201036](#)].
- [20] F. Krauss, R. Kuhn and G. Soff, *AMEGIC++ 1.0: A matrix element generator in C++*, JHEP **02** (2002), 044, [[hep-ph/0109036](#)].
- [21] T. Gleisberg et al., *Helicity formalism for spin-2 particles*, JHEP **09** (2003), 001, [[hep-ph/0306182](#)].
- [22] S. Jadach and B. F. L. Ward, *YFS2: The second order Monte Carlo for fermion pair production at LEP/SLC with the initial state radiation of two hard and multiple soft photons*, Comput. Phys. Commun. **56** (1990), 351–384.
- [23] F. A. Berends, W. L. van Neerven and G. J. H. Burgers, *Higher Order Radiative Corrections at LEP Energies*, Nucl. Phys. **B297** (1988), 429.
- [24] W. Placzek and S. Jadach, *Multiphoton radiation in leptonic W-boson decays*, Eur. Phys. J. **C29** (2003), 325–339, [[hep-ph/0302065](#)].
- [25] C. Amsler et al., Particle Data Group collaboration, *Review of particle physics*, Phys. Lett. **B667** (2008), 1.
- [26] S. Jadach, *Monte-Carlo Methods for High-Energy Physics, Lectures at the Torino School of Physics, 2001*, <http://jadach.home.cern.ch/jadach/>.
- [27] R. Kleiss and W. J. Stirling, *Massive multiplicities and Monte Carlo*, Nucl. Phys. **B385** (1992), 413–432.
- [28] F. E. Low, *Bremsstrahlung of very low-energy quanta in elementary particle collisions*, Phys. Rev. **110** (1958), 974–977.
- [29] R. P. Feynman, *Space-time approach to quantum electrodynamics*, Phys. Rev. **76** (1949), 769–789.
- [30] V. N. Gribov, *Bremsstrahlung of hadrons at high energies*, Sov. J. Nucl. Phys. **5** (1967), 280.
- [31] M. Chaichian and B. Ermolaev, *Factorization theorem for photons and gluons in hard processes*, Nucl. Phys. **B451** (1995), 194–206.
- [32] W. J. Marciano and A. Sirlin, *Deviations from electron-muon universality in the leptonic decays of the intermediate bosons*, Phys. Rev. **D8** (1973), 3612–3615.
- [33] S. Jadach and B. F. L. Ward, *Renormalization group improved Yennie-Frautschi-Suura theory and monte carlo event generators*, Contributed to 1987 Int. Symp. on Lepton and Photon Interactions at High Energies, Hamburg, West Germany, Jul 27-31, 1987.

- [34] S. Jadach, *Yennie-Frautschi-Suura soft photons in Monte Carlo event generators*, MPI-PAE/PTh 6/87.
- [35] P. Golonka and Z. Was, *PHOTOS Monte Carlo: A precision tool for QED corrections in Z and W decays*, Eur. Phys. J. **C45** (2006), 97–107, [[hep-ph/0506026](#)].